



1 **Characterization of atmospheric trace gases and particle matters in** 2 **Hangzhou, China**

3 Gen Zhang¹, Honghui Xu², Bing Qi³, Rongguang Du³, Ke Gui¹, Hongli Wang⁴, Wanting Jiang⁵, Linlin
4 Liang¹, Wanyun Xu¹

5 ¹State Key Laboratory of Severe Weather & Key Laboratory of Atmospheric Chemistry of CMA, Chinese Academy of
6 Meteorological Sciences, Beijing 100081, China

7 ²Zhejiang Institute of Meteorological Science, Hangzhou 310008, China

8 ³Hangzhou Meteorological Bureau, Hangzhou 310051, China

9 ⁴State Environmental Protection Key Laboratory of Formation and Prevention of Urban Air Pollution Complex, Shanghai
10 Academy of Environmental Sciences, Shanghai 200233, China

11 ⁵Plateau Atmospheric and Environment Laboratory of Sichuan Province, College of Atmospheric Science, Chengdu
12 University of Information Technology, Chengdu 610225, China

13 *Correspondence to:* Gen Zhang (zhangg@camsma.cn) and Honghui Xu (forsnow@126.com)

14 **Abstract.** The Yangtze River Delta (YRD) is one of the most densely populated regions in China with severe air quality
15 issues, which has not been fully understood. Thus, in this study, based on one-year (2013) continuous measurement at a
16 National Reference Climatological Station (NRCS, 30.22°N, 120.17°E, 41.7 m a. s. l) in the center of Hangzhou in the YRD,
17 we investigated the seasonal characteristics, interspecies relationships, and the local emissions and the regional potential
18 source contributions of trace gases (including O₃, NO_x, NO_y, SO₂ and CO) and particulate matters (PM_{2.5} and PM₁₀). Results
19 revealed severe two-tier air pollution (photochemical and haze pollution) occurred in this region, with frequent exceedances
20 in O₃ (38 days) and PM_{2.5} (62 days). O₃ and PM_{2.5} both exhibited distinct seasonal variations with reversed patterns: O₃
21 reaching a maximum in warm seasons (May and July) but PM_{2.5} in cold seasons (November to January). The overall results
22 from interspecies correlation indicated a strong local photochemistry favoring the O₃ production under a volatile organic
23 compound (VOC)-limited regime, whereas it moved towards an optimum O₃ production zone during warm seasons,
24 accompanying with a formation of secondary fine particles under high O₃. The emission maps of PM_{2.5}, CO, NO_x, and SO₂
25 demonstrated that local emissions were both significant for these species on seasonal scale. The contributions from the
26 regional transports among inland cities (Zhejiang, Jiangsu, Anhui, and Jiangxi Province) on seasonal scale were further
27 confirmed to be crucial to air pollution at NRCS site by using the backward trajectories simulations. Air masses transported
28 from Yellow Sea, East Sea, and South Sea were also found to be highly relevant to the elevated pollutants, especially for
29 NO_x and O₃. Case studies of photochemical pollution (O₃) and haze (PM_{2.5}) episodes both suggested the combined
30 importance of local atmospheric photochemistry and synoptic conditions during the accumulation (related with anticyclones)
31 and dilution process (related with cyclones). This study supplements a general picture of the air pollution state in the YRD



32 region, specifically elucidates the role of local emission and regional transport, and interprets the physical and photochemical
33 processes during haze and photochemical pollution episodes. Moreover, this work suggests that cross-regional control
34 measures are crucial to improve air quality in the YRD region, and further emphasizes the importance of local thermally
35 induced circulation on air quality.

36 1 Introduction

37 Ambient air quality is mainly affected by particle matters and gaseous pollutants such as ozone (O_3), nitrogen oxides (NO_x),
38 carbon monoxide (CO), and sulfur dioxide (SO_2). Particle matters ($PM_{2.5}$ and PM_{10}) are both from natural sources (e.g.,
39 windborne dust, volcanoes) or anthropogenic activities such as fossil and biomass fuel combustion (Chow and Watson,
40 2002). They have received extensive attention due to their harmful impact not only on human health such as aggravating
41 chronic respiratory and cardiovascular diseases (Pope et al., 1999) but also on climate change (Seinfeld et al., 2004; IPCC,
42 2007; Mercado et al., 2009). As primary gaseous pollutants, NO_x , CO, and SO_2 are all trace gases and derived from the
43 anthropogenic activities (Kato and Akimoto, 1994; Streets and Waldhoff, 2000). NO_x , with a short lifetime, is mainly
44 emitted from the fuel burning in the polluted region. In contrast, CO has a relatively long atmospheric lifetime and emitted
45 from the combustion sources, thus it's also a preferred tracer for indicating the anthropogenic pollution and charactering the
46 other pollutants (Jaffe et al., 1997; Parrish et al., 1998). In addition to the net downward transport of O_3 by eddy diffusion
47 from the stratosphere aloft, tropospheric O_3 is a well-known secondary gaseous pollutants and formed through the
48 photochemical oxidation of volatile organic compounds (VOCs) and nitrogen oxides (NO_x) under the irradiation of sunlight
49 (Logan, 1985; Roelofs et al., 1997), which has been also increasingly concerned with its adverse effect on exacerbating
50 chronic respiratory diseases and causing short-term reductions in lung function (Shao et al., 2006; Streets et al., 2007; Liu et
51 al., 2013) and vegetation (Feng et al., 2014). Reactive nitrogen (NO_y) is defined as the sum of NO_x and all compounds that
52 are products of the atmospheric oxidation of NO_x (e.g., PANs, HNO_3 , and HONO). Except NO_x , the other constituents in
53 NO_y are also mainly produced via the complex conversions within primary gaseous pollutants (i.e., photochemical oxidation
54 and nighttime chemistry). Moreover, some critical interactions have been verified existing between the gaseous pollutants
55 and or particle matters (Zhang et al., 2004; Cheng et al., 2016). For instance, in the presence of high NH_3 and low air
56 temperature, ammonium nitrate (NH_4NO_3) is formed in regions with HNO_3 and NH_3 , which is an important constituent of
57 $PM_{2.5}$ under the high NO_x condition (Seinfeld and Pandis, 2006). To some extent, such interactions further improve or
58 deteriorate the air quality. The oxidation of SO_2 can lead to acid deposition but also contributes to the formation of sulphate
59 aerosols (Meagher et al., 1978; Saxena and Seigneur, 1987), which in turn will influence the solar radiation and
60 photochemistry (Dickerson et al., 1997) and further weaken the formation of secondary pollutants. Therefore, clear
61 understanding in their characteristics, sources, transport, and formation mechanisms including interactions is crucial for
62 gaining the comprehensive information on the complex air pollution.

63 The Yangtze River Delta (YRD) region is located in the eastern of China, including the mega-city Shanghai and the well-
64 industrialized areas of southern Jiangsu Province and northern Zhejiang Province, with over ten large cities such as



65 Hangzhou, Suzhou, Wuxi and Changzhou lying along the mid-YRD (Fig. 1). Being one of the most rapid growths of
66 transportation, industries, and urbanization regions in China, it has been became hot spot with air pollution problems over
67 the past three decades, together with the Pearl River Delta (PRD) and Beijing-Tianjin-Hebei (BTH) region. To date,
68 numerous combined studies of O₃ and PM_{2.5} were implemented in representative urban cities in YRD region such as
69 Shanghai (Geng et al., 2007; Ding et al., 2013; Li et al., 2016a; Miao et al., 2017a) and Nanjing (Wang et al., 2002; Wang et
70 al., 2003; Kang et al., 2013; Chen et al., 2016). On the contrary, in Hangzhou (29.25°-30.5°N, 118.34°-120.75°E), a capital
71 city of Zhejiang Province in YRD region, which is lying along the mid-YRD, only a few sole studies of PM_{2.5} or O₃ were
72 sporadically conducted. To our knowledge, the pioneer measurement of O₃ in or around Hangzhou started in the 1990s at
73 Lin'an site, a regional station located in the east Zhejiang Province (50 km away from Hangzhou) (Luo et al., 2000).
74 Subsequent studies at this site depicted the first picture of the seasonal variations of O₃ and its precursors (Wang et al., 2001;
75 Wang et al., 2004). Xu et al. (2016) concluded the medium long range boundary transport of air masses coming from
76 biomass burning regions was responsible for the formation of haze aerosols at Lin'an site during the winter. In the urban
77 Hangzhou, Li et al (2017) recently reported the results of short-term measurements of O₃, CO, and non-methane
78 hydrocarbons at three sites in Hangzhou in the summertime of 2013. In terms of particle matters, Wu et al. (2016a) reported
79 that the local vehicle emission was a major contribution to PM_{2.5}, while results from Yu et al. (2014) suggested cross-border
80 transports rather than local emissions control high PM_{2.5} concentration and formation. Hence, large knowledge gap and
81 discrepancy still exist in understanding the complex combined pollution of O₃ and PM_{2.5} in Hangzhou.

82 To supplement the picture of air pollution in the YRD, we conducted continuous measurements of trace gases (O₃, NO_x,
83 NO_y, CO, and SO₂) and particle matters (PM_{2.5} and PM₁₀) during January-December 2013 at a regional site NRCS (National
84 Reference Climatological Station) in Hangzhou, which is also an integrated measurement site for the research of climate
85 change and atmospheric environment. This study presents the first results of one-year measurements of trace gases and
86 particle matters in the urban area of Hangzhou, investigates the characteristics and cause of these chemicals by discussing
87 their seasonal characteristics, interspecies correlations, the concentration dependence on local emission and regional
88 transport, and the specific photochemical pollution and haze case, respectively.

89 2 Introduction to the experiment, meteorological conditions, and methodology

90 2.1 Site description

91 Hangzhou is situated in the eastern coast of China and is one of the most developed cities in the Yangtze River Delta region.
92 It has 8.9 million population and 2.7 million vehicles according to the 2014 Statistical Bulletin of Hangzhou. It belongs to
93 the subtropical monsoon climate, with an average temperature of 17.0°C, relative humidity of 75% and rainfall of 1438 mm
94 over the past 30 years (1981-2010). In this study, all in-situ measurements of gaseous constituents, particles and
95 meteorological factors were conducted at NRCS site (30.22°N, 120.17°E, 41.7 m a.s.l) in the center of Hangzhou (Fig. 1). As
96 the right top map shown in Fig. 1, the site is adjacent to Prince Bay Park (area, 0.8 km²) and situated in the northeastern of



97 West Lake famous scenic spot (area, 49 km²) and commercial and residential areas in the south of city. There are no local
98 industrial pollution sources around the site. Thus, all gaseous constituents at this site can be representative of the urban areas
99 in Hangzhou.

100 2.2 Measurements description

101 Measurements of trace gases, aerosols, and meteorological parameters were conducted at NRCS station during January-
102 December 2013. Trace gases including O₃, SO₂, NO, NO_y, and CO were detected by a set of commercial trace gas analyzers
103 (Thermo Environmental Instruments Inc., USA i-series 49i, 43i, 42i, 42i-Y, and 48i), respectively, with a resolution of 1 min.
104 All the instruments are housed on the top floor of a laboratory building, which sits on the top of a hill about 40 m above the
105 ground level. Ambient air was drawn from the 1.5 m above the rooftop to the laboratory building through a manifold
106 connected to O₃, SO₂, NO and CO analyzers with PFA Teflon tubes (inside diameter: 2 cm). A separate sample line with a
107 MoO converter was used for NO_y analyzer. All trace gas analyzers were weekly span and daily zero checked, and multi-
108 point calibration was made once a month.

109 Ambient PM_{2.5} samples were collected using co-located Thermo Scientific (formerly R&P) Model 1405D samplers. The
110 sensor unit contains the two mass measurement hardware systems that monitor particles that continuously accumulate on the
111 system's exchangeable TEOM filters. PM-Coarse and PM_{2.5} particulate, split by a virtual impactor, each accumulate on the
112 system's exchangeable TEOM filters. By maintaining a flow rate of 1.67 L·min⁻¹ through the coarse sample flow channel
113 and 3 L·min⁻¹ through the PM_{2.5} sample channel, and measuring the total mass accumulated on each of the TEOM filters, the
114 device can calculate the mass concentration of both the PM_{2.5} and PM Coarse sample streams in near real-time. TEOM filters
115 must be replaced before the filter loading percentage reaches 80% to ensure the quality of the data generated by the
116 instrument. For PM, the precisions of this instrument were 2.0 µg cm⁻³ for 1 h average and 1.0 µg cm⁻³ for 24 h average.

117 2.3 Meteorological characteristic

118 Table 1 shows the monthly averaged meteorological parameters at NRCS station, suggesting distinct characteristics of air
119 temperature in winter and summer in this region, with monthly averages from ca. 5 °C in January to ca. 32 °C in July. High
120 relative humidity (RH) and a large amount of rainfall appeared in June (346 mm in total), and oppositely less precipitation
121 and low RH in autumn and winter. Note that the seemed high RH and large rainfall occurred in October was due to an
122 extremely synoptic event on 7 October, 2013 with the daily total rainfall of 91 mm. In addition, the wind rose implied that
123 the prevailing wind was from northwest in autumn, north in winter, and from southwest in spring and summer (See Fig. S1
124 in the Supplement).

125



126 2.4 Methodology

127 2.4.1 Air mass back trajectory cluster

128 In this study, 72-h back trajectories starting at the arrival level of 100 m from NRCS sites were calculated by using the
 129 National Oceanic and Atmospheric Administration (NOAA) HYSPLIT-4 model with a $1^\circ \times 1^\circ$ grid and the final
 130 meteorological database. The six hourly final archive data were obtained from the National Center for Environmental
 131 Prediction's Global Data Assimilation System (GDAS) wind field reanalysis. GDAS uses a spectral medium-range forecast
 132 model. More details could be showed at <http://www.arl.noaa.gov/ready/open/hysplit4.html>. The model was run four times
 133 per day at starting times of 00:00, 6:00, 12:00, and 18:00 UTC (08:00, 14:00, 20:00, and 02:00 LT, respectively). The
 134 method used in trajectory clustering was based on the GIS-based software TrajStat (Wang et al. 2004).

135 2.4.2 Potential source contribution function

136 The potential source contribution function (PSCF) is widely used to identify regional sources based on the HYSPLIT model.
 137 The zone of concern is divided into $i \times j$ small equal grid cells. The PSCF value in the ij -th cell is defined as m_{ij}/n_{ij} , where n_{ij}
 138 is denoted as the numbers of endpoints that fall in the ij -th cell and m_{ij} represents the numbers of "polluted" trajectory
 139 endpoints in the ij -th cell. In this analysis, average concentrations were considered as the "polluted" threshold (Hsu et al.,
 140 2003; Zhang et al., 2013). To minimize the effect of small values of n_{ij} , following the method of Polissar et al. (1999), the
 141 seasonal PSCF values were multiplied by arbitrary seasonal weight functions W_{ij} , expressed by WPSCF, to better reflect the
 142 uncertainty in the values for these cells. Geographic areas covered by more than 95% of the back trajectories are selected as
 143 the study domain. In this study, our study domain was in the range of 15 - 55°N and 105 - 135°E . The resolution was $0.5^\circ \times 0.5^\circ$.

$$144 \quad W_{ij(\text{spring})} = \begin{cases} 1.00 & 36 < n_{ij} \\ 0.70 & 12 < n_{ij} \leq 36 \\ 0.42 & 6 < n_{ij} \leq 12 \\ 0.17 & n_{ij} \leq 6 \end{cases} \quad W_{ij(\text{summer})} = \begin{cases} 1.00 & 42 < n_{ij} \\ 0.70 & 14 < n_{ij} \leq 42 \\ 0.42 & 7 < n_{ij} \leq 14 \\ 0.17 & n_{ij} \leq 7 \end{cases}$$

$$145 \quad W_{ij(\text{autumn})} = \begin{cases} 1.00 & 36 < n_{ij} \\ 0.70 & 12 < n_{ij} \leq 36 \\ 0.42 & 6 < n_{ij} \leq 12 \\ 0.17 & n_{ij} \leq 6 \end{cases} \quad W_{ij(\text{winter})} = \begin{cases} 1.00 & 54 < n_{ij} \\ 0.70 & 18 < n_{ij} \leq 54 \\ 0.42 & 9 < n_{ij} \leq 18 \\ 0.17 & n_{ij} \leq 9 \end{cases}$$

146 Moreover, to better elucidate the local and regional contribution to pollutants concentrations, we further compared the
 147 WPSCF results with their corresponding emission inventories of $\text{PM}_{2.5}$, CO , NO_x , and SO_2 in 2013 provided by Peking
 148 University (<http://inventory.pku.edu.cn/>), which were estimated by using a bottom-up approach with $0.1^\circ \times 0.1^\circ$ spatial
 149 resolution (Wang et al., 2013; Huang et al., 2014; Zhong et al., 2014), respectively.



150 2.4.3 Geopotential height (GH)

151 The geopotential height (GH) fields derived from the National Center for Environmental Prediction (NCEP) global Final
152 (FNL) reanalysis (<http://rda.ucar.edu/datasets/ds083.2/>) are typically used to classify the synoptic types (Miao et al., 2017b).
153 In this study, daily GH fields at the 925 hPa level from the NCEP-FNL reanalysis covering the region (100-135 °E, 20-50 °N)
154 were classified to the prevailing synoptic types during photochemical pollution and haze episodes as discussed in Section 3.5.
155 The NCEP-FNL reanalysis was produced from the Global Data Assimilation System, which continuously assimilates
156 observations from the Global Telecommunication System and other sources. The NCEP-FNL reanalysis fields were on $1^{\circ} \times 1^{\circ}$
157 grids with a 6 h resolution.

158 3 Results and discussion

159 3.1 Concentration levels

160 To evaluate the overall concentration level of gaseous and particle pollution at NRCS, we selected a Grade II standard of the
161 Chinese Ambient Air Quality Standards (CAAQS, GB 3095-2012), which was released in 2012 by the China State Council
162 and implemented thorough the whole nation in 2016 (MEP, 2012). Inferred from the Grade II CAAQS for $\text{PM}_{2.5}$ ($75 \mu\text{g m}^{-3}$
163 for 24 h average) and PM_{10} ($150 \mu\text{g m}^{-3}$ for 24 h average), 62 days and 26 days of $\text{PM}_{2.5}$ and PM_{10} exceedances with daily
164 average of $102.2 \mu\text{g m}^{-3}$ and $195.3 \mu\text{g m}^{-3}$ were classified thorough the period, respectively, mostly occurred in winter. For
165 O_3 , about 38 days exceedances (93 ppbv for 1 h average for the Grade II CAAQS) in whole were found during the whole
166 period, mostly covering from May to September. It suggested Hangzhou was suffering from heavy haze and photochemical
167 pollution in cold and warm seasons. Concerning SO_2 , the annual mean was 10.9 ppbv in this study, nearly half of the yearly
168 mean of SO_2 Grade II CAAQS (21 ppbv). It was reasonably attributed to the powerful measure of Chinese government to
169 control the emission of SO_2 starting at 1990 (He et al., 2002; Qi et al., 2012). Table 2 summarized a statistical analysis on
170 these species and listed the comparison with the previous results in other typical regions in China. In general, with respect to
171 all these chemicals, our results were generally comparable with those observed by other contemporaneous measurements in
172 Hangzhou and the other cities in YRD. As expected, regional differences between YRD, PRD, and BTH could be also found
173 as illustrated in Table 2. For instance, observed $\text{PM}_{2.5}$, PM_{10} , and CO concentrations were higher in BTH than those in YRD
174 and PRD through the comparison among provincial capital cities in China during 2011-2014 (Chai et al., 2014; Wang et al.,
175 2014), which has been extrapolated to be more emissions from coal-based industries and coal and biomass burning based
176 domestic home heating in BTH in winter (Zhang et al., 2012; Yang et al., 2013; Chai et al., 2014). Moreover, slight
177 decreases in $\text{PM}_{2.5}$ and PM_{10} at NRCS were both evidenced by their respective difference between 2013 and 2010-2011 (Tab.
178 2), coincident with the results derived from the satellite data and ground monitoring in China (Ma et al., 2016; Seltenrich,
179 2016). For NO_y , only rough comparison was implemented due to very limited measurements executed in China. The yearly
180 mean NO_y concentration of 63.7 ppbv in this study was slightly higher than 54.6 ppbv in Beijing (Wu et al., 2016b). It's
181 interestingly noted that slightly higher NO_y at NRCS possibly indicated more photochemical conversion of NO_x in



182 Hangzhou than Nanjing in the presence of nearly identical NO_2 . Additionally, the daytime mean concentrations were
183 comparable with those at nighttime for $\text{PM}_{2.5}$ nearly in all seasons but higher for O_3 due to the daily variations in solar
184 radiation and air temperature, the reverse is true for CO , NO_x , and NO_y .

185 3.2 Seasonal characteristics

186 Figure 2 shows seasonal variations of atmospheric O_3 (a), CO (b), NO (c), NO_x (d), NO_y (e), O_x (f), $\text{PM}_{2.5}$ (g), PM_{10} (h), and
187 SO_2 (i). Ozone exhibits a distinguished seasonal variation, with a board peak in late spring and middle summer (a maximum
188 in May and a secondary maximum in July) and a minimum in winter (November to January). Its observed behavior at NRCS
189 is different from what has been disclosed in previous studies conducted in southern and northern China, such as a summer
190 minimum and an autumn maximum of O_3 found in Hong Kong and an early summer (June) broad maximum recorded in
191 Beijing (Ding et al., 2008; Lin et al., 2008, 2009; Zhang et al., 2014). Recently, Ding et al. (2013) presented two peaks of O_3
192 appearing in summer (July) and early autumn (September) at Xinlin site in the suburban area northeast of Nanjing (about
193 239 km away from NRCS station). Regarding the geographical location of Hangzhou, which is upwind of the YRD under
194 the influence of southeasterly summer monsoon, the emissions in the YRD region and the solar radiation might be the main
195 causes of an O_3 formation in summer, resulting in a different seasonal cycle of O_3 compared to other continent sites in the
196 west/northwest YRD. In fact, the CO and NO_y data (Fig. 2b and Fig. 2e) show that these precursors were still at fairly high
197 levels (about 500 ppbv and 35 ppbv, respectively) in summer. The low O_3 level in winter, especially at night, can be
198 attributed to the lower temperature, weaker solar radiation, and in particular the strong destruction of O_3 by chemical titration
199 of NO from local emission or regional transport as discussed below (Lin et al., 2008, 2009, 2011). Note that, a slight drop of
200 O_3 was found in June compared with other months in summer, mainly attributing to the more frequent rainy days (23 days)
201 and larger rainfall in June (346 mm) than those in May (15 days) and July (5 days) during summertime (Table 1).

202 For $\text{PM}_{2.5}$ and PM_{10} , Fig. 2g and -2h both displayed overall well-defined seasonal variations with the maximum in winter
203 (December) and the minimum in summer (July). In cold seasons the emission of particulate matter is normally high due to
204 more emission of fossil fuels during heating in northern China (Zhang et al., 2009), which contributed to the enhancements
205 of particle matters and other tracer gases (i.e., CO and NO_x) at NRCS site via long-distance transport (See discussion in
206 Section 3.4). Furthermore, in winter temperature inversion and low mixing layer contribute to decrease particle suspension
207 and advection (Miao et al., 2015a). Also, dry/wet deposition should have strong seasonal variations because high
208 precipitation favors wet-deposition and high soil humidity, and the growth of deciduous plants may also favor the dry
209 deposition of particle matter in warm seasons (Zhang et al., 2001). The relatively low concentrations of $\text{PM}_{2.5}$ and PM_{10} in
210 summer may be also partly due to an increased vertical mixing (i.e., a higher boundary layer height) and more convection
211 (Ding et al., 2013; Miao et al., 2015b). $\text{PM}_{2.5}$ mass concentration also show strong month-to-month variations. The
212 simultaneous drop of $\text{PM}_{2.5}$ and PM_{10} concentrations together with other primary pollutants (i.e., SO_2 , CO and NO_y) in
213 February was mainly ascribed to the winter break of the Chinese Spring Festival, which started at the end of January and



214 lasted until mid-February. Notably, the seasonal pattern for PM was similar to NO_x , which suggested that traffic and heating
215 emissions were important to the $\text{PM}_{2.5}$ variation.

216 For other trace gases (CO , NO_x , NO_y , and SO_2), they all revealed clear seasonal variations but also some unique month-to-
217 month variation patterns (Fig. 2a-2f and Fig. 2i). Similar seasonal patterns among CO , NO_x , and SO_2 were generally found
218 with pronounced minimums appearing in summer and higher levels in fall and winter. Similar reasons with particle matters
219 could interpret these seasonal patterns such as the variation in the boundary layer height and the long-distance transport as
220 mentioned above. The last but not the least was photochemistry. During summer, it's most active to accelerate the
221 transformation of primary gaseous pollutants, whereas in winter, weaker photochemical reaction cannot remove the gases as
222 quickly as in the warmer seasons from the atmosphere.

223 NO_y concentration increased at the end of autumn, with a maximum in December together with a sharp peak of NO . Time
224 series implied that in December there was a multi-day episode of NO_x with high mixing ratios of NO and NO_2 both reaching
225 up to 100 ppbv and these days were generally correlated with northwest wind, suggesting a fresh emission from factories in
226 the industrial zone in the northwest. The "potential ozone" O_x ($\text{O}_3 + \text{NO}_2$) is usually used as an estimate of atmospheric total
227 oxidant (Lin et al., 2008). In summer (Fig. 2f), an abnormally high level of O_x (mainly as NO_2) was found in winter but for
228 O_3 decreased. The high level of NO_2 in O_x was expected to be originated from the significant titration of high NO by O_3 in
229 November and December (Fig. 2a).

230 As shown in Fig. 2i, SO_2 displayed a strong increase in winter but a significant drop in November. This pronounced
231 winter peaks were mainly due to the increased coal consumption for heating as mentioned above. The drop was associated
232 with the $\text{PM}_{2.5}$ maximum and a relatively high RH (Fig. 2g and Table 1), suggesting a possible role of heterogeneous
233 reactions (Ravishankara, 1997).

234 3.3 Inter-species correlations

235 Inter-species correlation could be normally used as an agent for acquiring some insights on their chemical formation,
236 removal processes, and interactions. As displayed in Fig. 3-7, we presented scatter plots of O_3 - NO_y , $\text{PM}_{2.5}$ - NO_y , SO_2 - NO_y ,
237 CO - NO_y , and $\text{PM}_{2.5}$ - O_3 correlations based on the whole dataset, respectively, and further discriminated these correlations
238 under typical environmental or meteorological impacts with color-coded parameters (i.e., relative humidity, air temperature,
239 and O_3 concentration). Clearly, overall negative correlation was found between O_3 and NO_y during the whole period (Fig. 3).
240 The color data showed that negative correlation mainly appeared with data of low air temperature, implying a remarkable
241 titration of freshly emitted NO with O_3 during the cold seasons and at nighttime. In contrast, a positive correlation between
242 O_3 and NO_y dominated under high air temperature, which usually occurred in the daytime of warm seasons within a
243 moderate level of NO_y (<150 ppbv). These findings suggested a strong local photochemical production of O_3 in summer,
244 leading to its seasonal variations as illustrated in Fig. 2a.

245 As illustrated in Fig. 4, a good positive correlation was found between $\text{PM}_{2.5}$ and NO_y , suggesting that $\text{PM}_{2.5}$ was highly
246 correlated with fossil combustion at this site. Some green data in the plot show very high NO_y concentration together with



247 low $PM_{2.5}$, suggesting that high NO air masses during December. Fig. 4 exhibited that high RH data were very scattered but
248 not very high $PM_{2.5}/NO_y$, implying that negligible interference of humidity on TEOM $PM_{2.5}$ measurement during the study
249 period, even under high RH condition in summer.

250 SO_2 and NO_y show a moderate to good correlation (See Fig. 5). Specifically, a better correlation and higher SO_2/NO_y ratio
251 were gained from air with low humidity. Nevertheless, the point distribution was much more scattered for the humid air
252 masses, and the ratio of SO_2/NO_y was clearly low, confirming a higher conversion of SO_2 to sulfate and/or deposition in the
253 humid condition (Khoder, 2002; Su et al., 2011). In this study, the averaged ratios of SO_2/NO_y during 18 February-30 April
254 was lower as 0.017, compared with that previously reported at Lin'an during the same months twelve years ago (Wang et al.,
255 2004). It was mainly owing to a remarkable reduction of SO_2 emission from power plants but an increased NO_x emission
256 associated with a huge consumption of petroleum fuels in the past decade in this region (Zhang et al., 2009).

257 Figure 6 shows a good positive correlation between CO and NO_y coded with O_3 mixing ratios. For CO lower than 3.2
258 ppmv during the whole period, an increase of NO_y generally led to lower O_3 concentrations, but CO reversed. As a
259 common origin of VOCs and CO, VOCs play a similar behavior with CO in the ozone photochemistry. Our results suggested
260 a VOCs-limited regime throughout the year in Hangzhou, consistent with the reported results in other cities of YRD region
261 (e.g., Shanghai and Nanjing) (Geng et al., 2007; Ding et al., 2013). While, as specifically shown in Fig. 6b, atmospheric O_3
262 (above 80 ppbv), mainly occurred in the afternoon (14:00-16:00 LT) in the summer and early autumn, exhibited increased
263 trend with the increasing NO_y within air masses with moderated CO mixing ratio of 0.25-1.5 ppmv, and the reversed trend
264 for CO was not expected to be significantly increased. It indicated that the transition from VOCs-limited regime to an
265 optimum O_3 production zone (even NO_x -limited regime), probably occurred at NRCS site in warmer seasons. We speculated
266 this change was mainly attributed to the larger emission of biogenic VOCs (BVOCs) compared to cold seasons. As reviewed
267 by Calafapietra et al. (2013), the VOC-limited conditions, in which O_3 production is limited by a high concentration of NO_x ,
268 are often observed in urban areas. However, if high BVOC emitters are common in urban areas, they could move the
269 VOC/ NO_x ratio toward optimal values for O_3 formation, and resulted in this ratio reaching in the city centers. As depicted in
270 Section 2.1, our study site is situated adjacent to Prince Bay Park (area, 0.8 km²) and in the northeastern of West Lake
271 famous scenic spot (area, 49 km²). For these two regions, they were both block green parks with high vegetation coverage.
272 Moreover, the primary tree species in these two regions are Liquidambar formosana and Cinnamomum camphora,
273 respectively, as major contributor to the emissions of isoprene and monoterpene (Chang et al., 2012), favoring the formation
274 of O_3 . Air masses from Prince Bay Park and West Lake famous scenic spot were confirmed to be transported to NRCS site
275 during warmer seasons, as illustrated in Fig. S1 and Fig. 8b. In addition to the strong temperature dependence of isoprenoid
276 emission (Guenther et al., 1995), a significantly increased emission of BVOCs was expected and thus it disturbed the
277 original balance between VOCs and NO_x relative to cold seasons. Our conclusion was generally in line with the
278 contemporaneous study implemented by Li et al. (2016a) who found that VOCs-limited regime accounted for 47% of the
279 ozone formation during the summer in Hangzhou, and the others are under NO_x -limited, taking BVOCs into consideration.



280 Recently, Li et al. (2017) also deduced the summer ozone mostly presented VOCs-limited and transition region alternately in
281 urban Hangzhou.

282 A scatter plot of O₃ with PM_{2.5} color-coded with air temperature was depicted in Fig. 7. During moderate to high air
283 temperature, a significant positive correlation was elucidated between O₃ and PM_{2.5} and the reverse negative correlation was
284 found under low temperature. The positive correlation for warm air probably reflected a formation of secondary fine
285 particles in summer associated with high O₃. The secondary particle formation may be related to high conversion rate of SO₂
286 to sulfate under a high concentration of oxidants (Khoder, 2002). Additionally, it was also associated with the formation of
287 secondary organic aerosols with high O₃ concentrations (Kamens et al., 1999; Lambe et al., 2015; Palm et al., 2017), which
288 was primarily produced through the photo-oxidation of BVOCs (Claeys, et al., 2004; Böge et al., 2013). As inferred above,
289 significant emission of BVOCs was speculated around NRCS in summer. The anti-correlation for cold air might be caused
290 by the titration effect of high NO concentration, which was in relation to high primary PM_{2.5} in cold seasons.

291 3.4 Dependences of pollutant concentrations on local emission and regional transport

292 To overview the impact of wind on the pollutants concentrations, we draw the seasonal wind dependence maps of pollutants
293 concentrations with wind sectors (See Fig. S2 in the Supplement for details). In total, similar seasonal patterns of wind
294 dependence map were found between CO and PM_{2.5}, SO₂, and NO_y (NO_x), in good agreement with their seasonal patterns as
295 shown in Section 3.2. For CO and PM_{2.5}, their top 10% concentrations were generally related with all the directions
296 throughout the year at speeds lower than 2 m s⁻¹ while bottom 10% were associated with others direction wind except north
297 at higher wind speed. It's necessary to pay attention on the scatter points of top 10% concentrations distributed in north
298 direction with high wind speed. With respect to the wind direction and transport, as the wind speed increases, pollutants
299 concentrations should have been decreasing due to the more effective local dilution, thus the increase instead might indicate
300 potential sources in these directions.

301 To address this issue and further investigate the relative contribution of local emission and regional transport, we
302 employed the trajectory clustering and WPSCF, along the comparison with the emission inventories. The 72 h back
303 trajectories from NRCS site were computed by using HYSPLIT model for four seasons. As shown in Fig. 9a, we obtained
304 six clusters by the clustering algorithm for four seasons with seven dominant paths distributed in east (E), northeast (NE),
305 north (N), northwest (NW), west (W), southwest (SW), and southeast (SE). The length of the cluster-mean trajectories
306 indicates the transport speed of air masses. In this analysis, the long and fast moving trajectories were disaggregated into
307 groups originating from more distant SE and SW regions during summer and NW and N regions during other seasons.
308 Member of this cluster have extremely long transport patterns, some of them even cross over Inner Mongolia and Mongolia
309 (e.g., N and NW). Trajectories belonging to S-SW and E-SE typically followed flow patterns from South Sea and Pacific
310 Ocean, respectively. Otherwise, some trajectories have short transport patterns, indicative of slow-moving air masses. Most
311 of the pollution episodes within this group are probably enriched from regional and local emission sources. Such trajectories
312 were also identified during every season in our study. For instance, the air masses associated with cluster 4 (in spring,



313 autumn, and winter) and cluster 1 in summer were predominantly originating from local areas and the nearby provinces with
314 significant pollution sources such as Jiangsu, Anhui, and Shanghai.

315 Table 3 summarizes the percentages of these identified trajectory clusters on seasonal basis and the corresponding mean
316 concentrations of PM_{2.5} and other trace gases related to each trajectory cluster. As inferred from Table 3, the clusters
317 exhibited larger variability and season dependence: the predominant clusters were W (42.66%) in spring, SW (53.89%) in
318 summer, NW (35.53%) in autumn, and N (54.91%) in winter, respectively. It's of interest to note that some trajectory
319 clusters with small percentages are remarkably related with high pollutants concentrations. In summer, a few PM_{2.5} pollution
320 cases (only 8.42% of the summertime trajectories) with mean concentration as high as 51.5 µg m⁻³ were related with the N
321 trajectories travelling across well-industrialized cities cluster (i.e., Suzhou, Wuxi, and Changzhou).

322 Furthermore, we depicted the seasonal WPSCF maps (a), the corresponding zoomed maps (b), and the emissions maps (c)
323 for PM_{2.5}, O₃, CO, NO_x, and SO₂, respectively, denoted with alphabets a, b, and c in the figure captions. Here we presented
324 the results of two representative species PM_{2.5} (Fig. 9a, -9b, and -9c) and O₃ (Fig. 10a, -10b) and those of the other species
325 were included in the Supplement (Fig. S3a, -S5c). Judging from the WPSCF maps, together with their corresponding
326 zoomed views and the calculated emissions maps, a few distinct features were summarized: (1) Local emissions were both
327 significant for the primary pollutants such as CO (Fig. S3), NO_x (Fig. S4), SO₂ (Fig. S5), and PM_{2.5} (Fig. 9) on seasonal scale.
328 For O₃, local photochemistry dominated during spring, summer, and autumn (Fig. 10a, -10b) due to strong photochemical
329 reactivity; (2) long transports from Yellow Sea, East Sea, and South Sea were also important potential sources for NO_x (Fig.
330 S4a) and O₃ (Fig. 10a, -10b); (3) The potential sources of CO and NO_x had similar patterns on spatial and seasonal scales,
331 with higher values in the NW during spring, covering the mid-YRD regions across Anhui Province and reaching the border
332 of Henan Province; in the NW and N during autumn and winter, covering the most area of Jiangsu Province and part of
333 Shandong Province such as Jinan, and Zibo city; (4) the higher values for SO₂ were located in the Ningbo city and the coast
334 of Yellow Sea during spring, in the southeastern region from East Sea during summer, probably due to ship emissions (Fan
335 et al., 2016), but in the inland cities such as Shaoxing and Quzhou city of Zhejiang Province during autumn and Anhui
336 Province during winter. In total, along with the air mass trajectories, the WPSCF maps for these primary pollutants were
337 generally in line with their respective corresponding species' emissions (Fig. 9c, -S3c, -S4c, and -S5c). Although no
338 seasonal patterns in emission maps were found, the emissions of these pollutants exhibited interspecies similarity and strong
339 spatial dependence with industrialization level. Note that the emission of NO_x was significant from South Korea (Fig. S4c)
340 where high WPSCF values were found in autumn (Fig. 10a), indicating a remarkable source to the surface O₃ of NRCS
341 through the northeasterly transport.

342 In terms of PM_{2.5}, the potential sources showed distinct seasonal variations such as southeastern regions of Jiangxi
343 Province and northwestern area of Zhejiang Province during spring and in the western city of North Korea (Pyongyang) and
344 South Korea (Seoul) with the northeasterly air mass across Yellow Sea during summer. As illustrated in Fig. 9a and -9b, the
345 contributions from local emission were both found to be more significant for autumn and winter than spring and summer,
346 covering all the cities in Zhejiang Province especially for the southern and southwestern part (e.g., Lishui, Jinhua, and



347 Quzhou city). Moreover, we found the higher WPSCF values located in the middle city of Jiangsu Province in autumn and
348 the expanded area towards the whole Jiangsu and Anhui Province and the southeast coast cities (e.g., Wenzhou, Ningbo in
349 Zhejiang Province, Fuzhou in Fujian Province) in winter, revealing the cross-boundary transport is crucial to the pollution of
350 particle matters. This result has been confirmed by Yu et al. (2014) who also found such transport dominated in the
351 Hangzhou city during the heavy haze episode (3-9 December, 2013).

352 For O₃, its potential sources exhibited distinct seasonal and spatial distributions: apart from the local contribution as
353 discussed above, the results with high WPSC values, as illustrated in Fig. 10a, indicated the main potential sources were
354 located in the western and southwestern region (e.g., Anhui, Jiangxi, and mid-Guangdong Province), and the northwestern
355 area such as Jiangsu, Henan, and Shandong Province during spring; In summer, more extensive potential sources were
356 elucidated to be located in the eastern-southern-southwestern regions of China, covering the southern part of Zhejiang
357 Province, southeastern cities of Jiangxi Province, almost the whole Fujian Province, and the eastern part of Guangdong
358 Province; the mid-Zhejiang Province (e.g., Quzhou, jinhua, and Ningbo city) and the northern coastal cities (e.g., Shanghai,
359 Lianyungang, and Dalian city) were apparently potential sources in autumn; in regard to winter, long distant transport acted
360 as a significant source of surface O₃, specifically from the northeasterly air mass Yellow Sea. A very interesting finding
361 should be pointed out that offshore area of East China Sea, Yellow China Sea, or even far from South China, respectively on
362 southeastern Zhejiang, Jiangsu, and Fujian Province were significant sources of O₃ at NRCS site throughout the year. We
363 speculated the recirculation of pollutants by sea- and land-breeze circulations around the cities along the YRD and Hangzhou
364 Bay which has been confirmed by Li et al. (2015, 2016b), was largely responsible for the increased concentration of O₃ at
365 NRCS site. Such an increase in O₃ concentrations in urbanized coastal areas have been observed and modeled in a number of
366 studies (Oh et al., 2006; Levy et al., 2008; Martins et al., 2012). Thus, our study further emphasizes the importance of local
367 thermally induced circulation on air quality.

368 3.5 Cases studies for haze (high PM_{2.5}) and photochemical pollution (high O₃) episodes

369 To elucidate the specific causes of high PM_{2.5} and O₃ episodes including the transport and local photochemical formation, we
370 chose two typical cases for detailed interpretations and are presented here. In this study, the haze pollution episode is defined
371 as the event that continuous days with daily averaged PM_{2.5} concentration exceeding 75 μg m⁻³, which has been also used to
372 distinguish non-haze and haze episode in other studies (Yu et al., 2014; Wu et al., 2016a). With respect to this campaign,
373 there were two non-haze episodes (Phase I (28 Nov.-3 Dec.), II (10-12 Dec.)), and their subsequent severe haze pollution
374 episodes (Phase III (2-9 Dec.) and IV (13-15 Dec.)) at NRCS site, respectively, as illustrated in Fig. 11. In the Phase III, it
375 showed that high PM_{2.5} (up to 406 μg m⁻³) appeared on 7 December and board PM_{2.5} peaks (around 300 μg m⁻³) occurred
376 before and after two days. Simultaneously, CO, SO₂, and NO_x also reached very high levels on this day, confirming that the
377 common origin of CO and PM_{2.5} from heating and combustion and the rapid conversion of SO₂ and NO_x to sulfate and
378 nitrate in PM_{2.5} in winter. But for O₃, its level reached as low as 11.5 ppbv at 15:00 LT on that day, owing to the weak
379 photochemical activity under the severe haze pollution. Along with the high NO₂ concentration (around 120 ppbv), it could



380 not produce sufficient conversion oxidants (OH and HO₂ radicals) for the gas-phase oxidation of SO₂ (Poppe et al., 1993;
381 Hua et al., 2008), while the increased relative humidity during 6-8 December possibly favored the aqueous phase oxidation
382 of SO₂.

383 Moreover, according to the results obtained from the backward trajectory cluster and WPSCF analysis during 2-9
384 December, 2013 (Fig. S6 in the Supplement), we found an apparent contribution from the transported air mass from
385 northwest region such as Jiangsu Province and Anhui Province. Our results were in good agreement with contemporaneous
386 measurement in Hangzhou (Wu et al., 2016a). Subsequently, at the end of this episode significant drops of these species
387 except O₃ were observed from 00:00 LT to 23:00 LT on 9 December (i.e., 189 to 41.6 μg m⁻³ for PM_{2.5}, 2.3 to 1.0 ppmv for
388 CO, and 145 to 47.9 ppbv for NO_x). Weather chart and wind data suggested that the region of NRCS was always controlled
389 by a strong continental high pressure system originating from northwest before 8 December (Fig. 12a-12f), but rapidly
390 changed to be dominated under a strong marine high pressure system coming from east at 02:00 LT on 9 December (Fig.
391 12g-12h), which brought clean maritime air passing over Yellow Sea and thus caused such decreases in these pollutants.
392 However, it quickly turned back to be controlled under a continental high pressure system described above, carrying
393 pollutants from the city clusters to the NRCS site. It could account for the accumulations of these species during the
394 intermediate period (Phase II). For the subsequent Phase IV with high PM_{2.5} episode it was also found to be governed by a
395 stagnant high pressure over YRD region (Fig. S7).

396 For the photochemical pollution events, we selected three cases with O₃ exceedances during May-August according to
397 Grade II standard of CAAQS as depicted in Section 3.1. As displayed in Fig. 13, they were the Phase I (28-30 May and 20-
398 22 June) with rapid buildup and decrease of O₃ within 3 days, Phase II (9-12 July) representing a distinct accumulation
399 process of O₃ exceedances, and the Phase III (1-3 May, 20-22 May, and 9-11 August) with high O₃ levels within three
400 consecutive days. For 28 May in the Phase I, weather chart suggested that a strong anticlockwise cyclone located over YRD.
401 In this case, the cyclone (i.e., low pressure) caused favoring conditions, e.g., cloudy weather and high wind velocities, for
402 pollution diffusion. Then, a strong clockwise anticyclone from northwest, sweeping over cities cluster (i.e., Nanjing and
403 Shanghai), rapidly moved adjacent to NRCS site on 29 May. It carried the primary pollutants such as CO, SO₂, NO_x from
404 these megacities and secondary products (i.e., O₃ and some NO_z) were further produced via complex photochemical
405 reactions under such synoptic conditions. As orange shaded area shown in Fig. 13, the hourly maximums of O₃ and PM_{2.5}
406 were observed as high as 141.2 ppbv and 135.8 μg m⁻³ at 13:00 LT on 29 May. Following this day, the cyclone again
407 dominated this region and caused sudden decreased in atmospheric pollutants. Also, similar case was found during 20-22
408 June under such changes in synoptic weather. For Phase II (9-12 July), a typical accumulation process was observed with the
409 daily maximums of atmospheric pollutants increasing from 90.4 to 142.9 ppbv for O₃, 77.6 to 95.3 μg m⁻³ for PM_{2.5}, and
410 80.2 to 125.2 ppbv for NO_y, respectively. The examination of day-to-day 925-hPa synoptic chart derived from NECP
411 reanalysis suggested that high pressure system governed over YRD during 9-11 July, with southwesterly prevailing wind.
412 The air masses recorded at this site mainly came from the most polluted city clusters in the southwest (e.g. Zhejiang, Jiangxi,
413 and Fujian Province). Meanwhile, the stagnant synoptic condition (i.e., low wind speed) favored the accumulation of



414 primary pollutants such as CO and NO_x. For secondary pollutants O₃ and PM_{2.5}, they were also rapidly formed via
415 photochemical oxidation and further accumulated under such synoptic condition, together with continuous high-temperature
416 (daily mean around 33 °C). On 12 July, a typhoon (No. 7 Typhoon Soulik) moved to a location a few hundred kilometers
417 away from NRCS site, bringing southeasterly maritime air over YRD. Daily maximum O₃ reached at 142.8 ppbv at 12:00 LT
418 even with low concentration of precursors (i.e., 0.48 ppmv for CO and 16.0 ppbv for NO_x), suggesting high photochemical
419 production efficiency of O₃ in this region in summer. This phenomenon has been also found in the multi-day episode of high
420 O₃ in Nanjing during 20-21 July, 2011 (Ding et al., 2013). In this phase, PM_{2.5} mass concentration showed very good
421 correlation ($R = 0.79$, $p < 0.001$) with O₃ during the daytime (09:00-17:00 LT), possibly indicating a common origin of
422 BVOCs due to the significant vegetation emission as discussed above, in addition to high biomass production in the southern
423 part of the YRD (Ding et al., 2013). For Phase III (1-3 May, 20-22 May, and 9-11 August), there were most sunny days with
424 low wind speed and moderate/high air temperature which were both beneficial factors for photochemical formation of O₃,
425 together with sufficient precursors (NO_x and VOCs) in the summer and early autumn over YRD. For 1-3 May and 20-22
426 May, daily maximum T were moderate (around 25 °C versus 31 °C), while the daily maximums NO_x reached as high as 43-
427 95 ppbv and 50-90 ppbv, respectively, which both favoring the photochemical formation to produce the continuous high O₃
428 concentrations (daily maximums: 96-133 ppbv via 104-133 ppbv). The reverse case is also true during 9-11 August, on
429 which the daily maximum T and NO_x ranged from 40.6-41.4 °C and 33-44 ppbv, respectively, resulting in producing
430 continuously high O₃ from 98.8 ppbv to 130.5 ppbv.

431 **3.6 Photochemical age and ozone production efficiency during photochemical pollution and haze period**

432 Photochemical age is often used to express the extent of photochemistry, which can be estimated using some indicator such
433 as NO_x/NO_y (Carpenter et al., 2000; Lin et al., 2008, 2009, 2011; Parrish et al., 1992). Air masses with fresh emissions have
434 NO_x/NO_y close to 1, while lower NO_x/NO_y ratio for the photochemical aged air masses. In this study, for the haze events as
435 mentioned above, the average and maximum NO_x/NO_y ratios were as high as 0.80 and 0.99, respectively, indicating that
436 photochemical conversion of NO_x is not absent but fairly slow. It was well consistent with the largely weakened
437 photochemistry due to the low intensity of UV radiation in winter. In contrast, during the photochemical pollution period,
438 they were low as 0.53 and 0.14 for the average and minimum ratio. The simultaneous measurements of atmospheric O₃, NO_x,
439 and NO_y can provide an insight into calculating the ozone production efficiency (OPE) for different seasons. From the data
440 of O_x and NO_z, the ratio of $\Delta(O_x)/\Delta(NO_z)$ can be calculated as a kind of observation-based OPE (Trainer et al., 1993; Sillman,
441 2000; Kleinman et al., 2002; Lin et al., 2011;). In this study, the mean values of NO_z and O_x between 07:00-15:00 LT, were
442 used to calculate the OPE values through the linear regressions. In addition, these data were also confined to the sunny days
443 and the wind speed below 3 m s⁻¹, reflecting the local photochemistry as possible. The OPE value during the photochemical
444 pollution period (SOPE) as mentioned above was 1.99, generally within the reported range of 1-5 in the PRD cities, but
445 lower than 3.9-9.7 in summer Beijing (Chou et al., 2009; Ge et al., 2012). Meanwhile, the OPE value of 0.77 during the haze
446 period (HPOE) was also comparable with the reported value of 1.1 in winter in Beijing (Lin et al., 2011). The smaller winter



447 OPE value in Hangzhou might be ascribed to the weaker photochemistry and higher NO_x concentration. At high NO_x level,
448 OPE tends to decrease with the increased NO_x concentration (Ge et al., 2010; Lin et al., 2011). In Hangzhou, the NO_x level is
449 frequently higher than needed for producing photochemical O_3 , and excessive NO_x causes net O_3 loss rather than
450 accumulation. In this study, 75% of daily OPE values were negative, for which two factors could be accounted. To some extent,
451 due to the geographical location and unique climate characteristic for Hangzhou as depicted above, the interference of
452 unbeneficial meteorological condition existed in the formation of local O_3 deriving from photochemistry, i.e., strong wind,
453 frequent rainy days. The other one is because of the consumption of O_3 by excessive NO_x , which was also well confirmed by
454 the conclusion that Hangzhou was mostly in the VOCs-limited regime as discussed in Section 3.2. Such circumstance was
455 also observed at the rural site Gucheng in the NCP and in Beijing urban area (Lin et al., 2009, 2011). Taking the average of
456 SOPE of 1.99 and the average daytime increment of NO_z (ca. 20 ppbv), we estimated an average photochemical O_3
457 production of about 39.8 ppbv during photochemical pollution period. In contrast, the lower average photochemical O_3
458 production was estimated to be 10.78 ppbv during haze period based on HOPE, which might act as a significant source for
459 surface O_3 in winter in Hangzhou.

460 4 Conclusions

461 In this study, we presented an overview of one year measurements of trace gases (O_3 , CO, NO_x , NO_y , and SO_2) and particle
462 matters ($\text{PM}_{2.5}$ and PM_{10}) at National Reference Climatological Station in Hangzhou. The characteristics and cause of these
463 chemicals were investigated by their seasonal characteristics, along the comparison with the previous results in other regions
464 in China, interspecies correlations, and the concentration dependence on local emission and regional transport. Specific
465 photochemical pollution and haze case were studied in detail based on discussing the physical process and photochemical
466 formation (ozone production efficiency). The main findings and conclusions are summarized below:

467 a) Within one year study period, there were 38 days of O_3 exceedances and 62 days of $\text{PM}_{2.5}$ exceedances of the National
468 Ambient Air Quality Standards in China at the site, suggesting heavy air pollution in this region. In general, the
469 concentration levels of these chemicals were consistent with those observed by other contemporaneous measurements in
470 Hangzhou and the other cities in YRD, but lower than those in NCP. Distinct seasonal characteristics were found with a
471 board peak in late spring and middle summer and a minimum in winter for O_3 , while with maximum in winter and minimum
472 in summer for $\text{PM}_{2.5}$.

473 b) A positive O_3 - NO_y correlation was found for air masses with high air temperature in summer, suggesting a strong local
474 photochemical production of O_3 . In addition, correlation analysis shows an important conversion of SO_2 to sulfate and/or
475 deposition in the humid condition. CO- NO_y - O_3 correlation suggested a VOC-limited regime for the overall study period but
476 moved toward an optimum O_3 production zone during warm seasons. The positive correlation between O_3 and $\text{PM}_{2.5}$ under
477 high air temperature indicated a formation of secondary fine particles in warm seasons, respectively.

478 c) The results from the emission inventories of the primary pollutants such as $\text{PM}_{2.5}$, CO, NO_x , and SO_2 demonstrated that
479 local emissions were both significant for these species but without distinct seasonal variations. The major potential sources



480 of PM_{2.5} were located in the regions of southwesterly in spring, northwesterly and northeasterly in summer, and
481 northwesterly (the whole Jiangsu Province and Anhui Province) in autumn and winter, respectively. For CO and NO_x, they
482 showed similar patterns with northwestern regions covering the mid-YRD regions and Anhui Province during spring and in
483 the northwestern and northern regions including Jiangsu Province and part of Shandong Province during autumn and winter.
484 The distinct seasonal variation in SO₂ potential might be from southwestern and eastern region during spring and summer
485 but northwestern during autumn and winter. Air masses transported from Yellow Sea, East Sea, and South Sea were also
486 important in increasing surface O₃, probably due to the recirculation of pollutants by sea- and land-breeze circulations
487 around the cities along the YRD and Hangzhou Bay. This finding further emphasizes the importance of urban-induced
488 circulation on air quality.

489 d) Case studies for photochemical pollution and haze episodes both suggest the combined importance of local atmospheric
490 photochemistry and synoptic weather during the accumulation (related with anticyclones) and dilution process (related with
491 cyclones) of these episodes. The average photochemical O₃ productions were estimated to be 39.8 and 10.78 ppbv during
492 photochemical pollution and haze period, respectively, indicating local photochemistry might act as a significant source for
493 surface O₃ in winter in Hangzhou.

494 Our study further completes a picture of air pollution in the YRD, interprets the physical and photochemical processes
495 during haze and photochemical pollution episodes, and explores the seasonal and spatial variations in the potential sources of
496 these pollutants. Moreover, this work suggests the cross-region control measures are crucial to improve air quality in the
497 YRD region, and further emphasizes the importance of local thermally induced circulation on air quality.

498

499 **Acknowledgement.** This study is financially supported by National Natural Science Foundation of China (41505108 and
500 41775127), National Key Research and Development Program of China (2016YFC0202300), and Shanghai Key Laboratory
501 of Meteorology and Health (QXJK201501). The authors are especially grateful to Dr. Miao Yucong for the technical
502 supports in drawing a part of figures and discussions.

503 **References**

- 504 Böge, O., Mutzel, A., Linuma, Y., Yli-Pirilä, P., Kahnt, A., Joutsensaari, J., and Herrmann, H.: Gas-phase products and
505 secondary organic aerosol formation from the ozonolysis and photooxidation of myrcene, *Atmos. Environ.*, 79, 553-560,
506 2013.
- 507 Calfapietra, C., Fares, S., Manes, F., Morani, A., Sgrign, G., and Loreto, F.: Role of biogenic volatile organic compounds
508 (BVOC) emitted by urban trees on ozone concentration in cities: A review, *Environ. Poll.*, 183, 71-80, 2013.
- 509 Cao, J., Shen, Z., Chow, J. C., Qi, G., and Watson, J. G.: Seasonal variations and sources of mass and chemical composition
510 for PM₁₀ aerosol in Hangzhou, China, *Particuology*, 7, 161-168, 2009.



- 511 Carpenter, L. J., Green, T. J., Mills, G. P., Bauguitte, S., Penkett, S. A., Zanis, P., Schuepbach, E., Schmidbauer, N., Monks,
512 P. S., and Zellweger, C.: Oxidized nitrogen and ozone production efficiencies in the springtime free troposphere over
513 the Alps, *J. Geophys. Res.*, 105, 14547-14559, 2000.
- 514 Chai, F. H., Gao, J., Chen, Z. X., Wang, S. L., Zhang, Y. C., Zhang, J. Q., Zhang, H. F., Yun, Y. R., and Ren, C.: Spatial and
515 temporal variation of particulate matter and gaseous pollutants in 26 cities in China, *J. Environ. Sci.*, 26, 75-82, 2014.
- 516 Chang, J., Ren, Y., Shi, Y., Zhu, Y. M., Ge, Y., Hong, S. M., Jiao, L., Lin, F. M., Peng, C. H., Mochizuki, T., Tani, A., Mu,
517 Y., and Fu, C. X.: An inventory of biogenic volatile organic compounds for a subtropical urban-rural complex, *Atmos.*
518 *Environ.*, 56, 115-123, 2012.
- 519 Chen, T., He, J., Lu, X., She, J., and Guan, Z.: Spatial and temporal variations of PM_{2.5} and its relation to meteorological
520 factors in the urban area of Nanjing, China, *Int. J. Environ. Res. Pub. Heal.*, 13, 921, 2016.
- 521 Cheng, Y. F., Zheng, G. J., Wei, C., Mu, Q., Zheng, B., Wang, Z. B., Gao, M., Zhang, Q., He, K. B., Carmichael, G., Pöschl,
522 U., and Su, H.: Reactive nitrogen chemistry in aerosol water as a source of sulfate during haze events in China, *Sci.*
523 *Adv.*, 2, 12, 1-11, 2016.
- 524 Chou, C. K., Tsai, C. Y., Shiu, C. J., Liu, S. C., and Zhu, T.: Measurement of NO_y during campaign of air quality research in
525 Beijing 2006 (CAREBeijing-2006): implications for the ozone production efficiency of NO_x, *J. Geophys. Res.*, 114, 1,
526 328-334, 2009.
- 527 Chow, J. C. and Watson, J. G.: Review of PM_{2.5} and PM₁₀ apportionment for fossil fuel combustion and other sources by
528 the chemical mass balance receptor model, *Energy Fuels*, 16, 2, 222-260, 2002.
- 529 Claeys, M., Graham, B., Vas, G., Wang, W., Vermeylen, R., Pashynska, V., Cafmeyer, J., Guyon, P., Andreae, M. O.,
530 Artaxo, P., and Maenhaut, W.: Formation of secondary organic aerosols through photooxidation of isoprene, *Science*,
531 303, 5661, 1173-1176, 2004.
- 532 Dickerson, R. R., Kondragunta, S., Stenchikov, G., Civerolo, K. L., Doddridge, B. G., and Holben, B. N.: The Impact of
533 aerosols on solar ultraviolet radiation and photochemical pollution, *Science*, 278, 5339, 827-830, 1997
- 534 Ding, A. J., Wang, T., Thouret, V., Cammas, J.-P., and N'ed'elec, P.: Tropospheric ozone climatology over Beijing: analysis
535 of aircraft data from the MOZAIC program, *Atmos. Chem. Phys.*, 8, 1-13, 2008.
- 536 Ding, A. J., Fu, C. B., Yang, X. Q., Sun, J. N., Zheng, L. F., Xie, Y. N., Herrmann, E., Nie, W., Petäjä, T., Kerminen, V. M.,
537 and Kulmala, M.: Ozone and fine particle in the western Yangtze River Delta: an overview of 1 yr data at the SORPES
538 station, *Atmos. Chem. Phys.*, 13, 5813-5830, 2013.
- 539 Fan, Q., Zhang, Y., Ma, W., Ma, H., Feng, J., Yu, Q., Yang, X., Ng, S.K.W., Fu, Q., and Chen, L.: Spatial and seasonal
540 dynamics of ship emissions over the Yangtze River Delta and East China Sea and their potential environmental
541 influence, *Environ. Sci. Technol.*, 50, 1322-1329, 2016.
- 542 Feng, Z. Z., Sun, J. S., Wan, W. X., Hu, E. Z., and Calatayud, V.: Evidence of widespread ozone-induced visible injury on
543 plants in Beijing, China, *Environ. Pollut.*, 193, 296-301, 2014.



- 544 Ge, B. Z., Xu, X. B., Lin, W. L., and Wang, Y.: Observational study of ozone production efficiency at the Shangdianzi
545 regional background station, *Environ. Sci.*, 31, 7, 1444-1450, 2010 (In Chinese with English abstract).
- 546 Ge, B. Z., Xu, X. B., Lin, W. L., Li, J., and Wang, Z. F.: Impact of the regional transport of urban Beijing pollutants on
547 downwind areas in summer: ozone production efficiency analysis, *Tellus*, 64, 17348, 2012.
- 548 Geng, F. H., Zhao, C. S., Tang, X., Lu, G. L., and Tie, X. X.: Analysis of ozone and VOCs measured in Shanghai: A case study,
549 *Atmos. Environ.*, 41, 989-1001, 2007.
- 550 Guenther, A., Hewitt, C. N., Erickson, D., Fall, R., Geron, C., Graedel, T., Harley, P., Klinger, L., Lerdau, M., McKay, W.
551 A., Pierce, T., Scholes, B., Steinbrecher, R., Tallamraju, R., Taylor, J., and Zimmerman, P. L.: A global model of
552 natural volatile organic compound emissions, *J. Geophys. Res.*, 100, 8873-8892, 1995.
- 553 He, K. B., Huo, H., and Zhang, Q.: Urban air pollution in China: current status, characteristics, and progress, *Annu. Rev.*
554 *Energ. Env.*, 27, 397-431, 2002.
- 555 Hsu, Y. K., Holsen, T. M., and Hopke, P. K.: Comparison of hybrid receptor models to locate PCB sources in Chicago,
556 *Atmos. Environ.*, 37, 545-562, 2003.
- 557 Hua, W., Chen, Z. M., Jie, C. Y., Kondo, Y., Hofzumahaus, A., Takegawa, N., Chang, C. C., Lu, K. D., Miyazaki, Y., Kita,
558 K., Wang, H. L., Zhang, Y. H., and Hu, M.: Atmospheric hydrogen peroxide and organic hydroperoxides during
559 PRIDE-PRD'06, China: their concentration, formation mechanism and contribution to secondary aerosols, *Atmos.*
560 *Chem. Phys.*, 8, 6755-6773, 2008.
- 561 Huang Y., Shen H. Z., Chen H., Wang R., Zhang Y. Y., Su S., Chen Y. C., Lin N., Zhao S. J., Zhong Q. R., Wang X. L., Liu
562 J. F., Li B. G., Liu W. X., and Tao S.: Quantification of global primary emissions of PM_{2.5}, PM₁₀, and TSP from
563 combustion and industrial process sources, *Environ. Sci. Technol.*, 48, 13834-13843, 2014.
- 564 IPCC, Summary for Policymakers. In *Climate Change 2007: The Physical Science Basis. Contribution of Working Group I*
565 *to the Fourth Assessment Report of the Intergovernmental Panel on Climate Change*; Solomon, S., Qin, D., Manning,
566 M., Chen, Z., Marquis, M., Averyt, K. B., Tignor, M., Miller, H. L., Eds.; Cambridge University Press: Cambridge,
567 United Kingdom and New York, NY, USA, 2007.
- 568 Jaffe, D. A., Mahura, A., Kelley, J., Atkins, J., Novelli, P. C., and Merrill, J.: Impact of Asian emissions on the remote North
569 Pacific atmosphere: interpretation of CO data from Shemya, Guam, Midway, and Mauna Loa, *J. Geophys. Res.*, 101,
570 2037-2048, 1997.
- 571 Kamens, R., Jang, M., Chien, C.J., and Leach, K.: Aerosol formation from reaction of α -pinene and ozone using a gas-phase
572 kinetics-aerosol partitioning model, *Environ. Sci. Technol.*, 33, 1430-1438, 1999.
- 573 Kang, H., Zhu, B., Su, J., Wang, H., Zhang, Q., and Wang, F.: Analysis of a long-lasting haze episode in Nanjing, China,
574 *Atmos. Res.*, 120-121, 78-87, 2013.
- 575 Kato, N. and Akimoto, H.: Anthropogenic emissions of SO₂ and NO_x in Asia: emission inventories, *Atmos. Environ.*, 26, 19,
576 2997-3017, 1994.



- 577 Khoder, M. I.: Atmospheric conversion of sulfur dioxide to particulate sulfate and nitrogen dioxide to particulate nitrate and
578 gaseous nitric acid in an urban area, *Chemosphere*, 49, 675–684, 2002.
- 579 Kleinman, L., Daum, P. H., Lee, Y.-N., Nunnermacker, L. J., Springston, S. R., Weinstein-Lloyd, J., and Rudolph, J.: Ozone
580 production efficiency in an urban area, *J. Geophys. Res.*, 107, 4733, 2002.
- 581 Lambe, A. T., Chhabra, P. S., Onasch, T. B., Brune, W. H., Hunter, J. F., Kroll, J. H., Cummings, M. J., Brogan, J. F.,
582 Parmar, Y., Worsnop, D. R., Kolb, C. E., and Davidovits, P.: Effect of oxidant concentration, exposure time, and seed
583 particles on secondary organic aerosol chemical composition and yield, *Atmos. Chem. Phys.*, 15, 3063-3075, 2015.
- 584 Levy, I., Dayan, U., and Mahrer, Y.: A five-year study of coastal recirculation and its effect on air pollutants over the east
585 Mediterranean region, *J. Geophys. Res.*, 113, D16121, 2008.
- 586 Li, M. M., Mao, Z. C., Song, Y., Liu, M. X., and Huang, X.: Impact of the decadal urbanization on thermally induced
587 circulations in eastern China, *J. Appl. Meteorol. Clim.*, 54, 259-282, 2015.
- 588 Li, L., An, J. Y., Shi, Y. Y., Zhou, M., Yan, R. S., Huang, C., Wang, H. L., Lou, S. R., Wang, Q., Lu, Q., and Wu, J.: Source
589 apportionment of surface ozone in the Yangtze River Delta, China in the summer of 2013, *Atmos. Environ.*, 144, 194-
590 207, 2016a.
- 591 Li, M. M., Song, Y., Mao, Z. C., Liu, M. X., and Huang, X.: Impact of thermal circulations induced by urbanization on
592 ozone formation in the Pearl River Delta, China, *Atmos. Environ.*, 127, 382-392, 2016b.
- 593 Li, K. W., Chen, L. H., Ying, F., White, S. J., Jang, C., Wu, X. C., Gao, X., Hong, S. M., Shen, J. D., Azzi, M., and Cen, K.
594 F.: Meteorological and chemical impacts on ozone formation : A case study in Hangzhou, China, *Atmos. Res.*, doi:
595 10.1016/j.atmosres.2017.06.003, 2017.
- 596 Lin, W. L., Xu, X. B., Zhang, X. C., and Tang, J.: Contributions of pollutants from North China Plain to surface ozone at the
597 Shangdianzi GAW Station, *Atmos. Chem. Phys.*, 8, 5889-5898, 2008.
- 598 Lin, W. L., Xu, X. B., Ge, B. Z., and Zhang, X. C.: Characteristics of gaseous pollutants at Gucheng, a rural site southwest
599 of Beijing, *J. Geophys. Res.*, 114, 4723-4734, 2009.
- 600 Lin, W. L., Xu, X. B., Ge, B. Z., and Liu, X.: Gaseous pollutants in Beijing urban area during the heating period 2007-2008:
601 variability, sources, meteorological, and chemical impacts, *Atmos. Chem. Phys.*, 11, 8157-8170, 2011.
- 602 Liu, T., Li, T. T., Zhang, Y. H., Xu, Y. J., Lao, X. Q., Rutherford, S., Chu, C., and Luo, Y.: The short-term effect of ambient
603 ozone on mortality is modified by temperature in Guangzhou, China, *Atmos. Environ.*, 76, 59-67, 2013.
- 604 Logan, J. A.: Tropospheric ozone: Seasonal behavior, trends, and anthropogenic influence. *J. Geophys. Res.*, 90, 10463-
605 10482, 1985.
- 606 Luo, C., St. John, J. C., Xiuji, Z., Lam, K. S., Wang, T., and Chameides, W. L.: A nonurban ozone air pollution episode over
607 eastern China: observations and model simulations, *J. Geophys. Res.*, 105, 1889-1908, 2000.
- 608 Ma, Z. W., Hu, X. F., Sayer, A. M., Levy, R., Zhang, Q., Xue, Y. G., Tong, S. L., Bi, J., Huang, L., and Liu, Y.: Satellite-
609 based spatiotemporal trends in PM_{2.5} concentrations: China, 2004-2013, *Environ. Health Persp.*, 124, 184-192, 2016.



- 610 Martins, D. K., Stauffer, R. M., Thompson, A. M., Knepp, T. N., and Pippin, M.: Surface ozone at a coastal suburban site in
611 2009 and 2010: relationships to chemical and meteorological processes, *J. Geophys. Res.*, 117, D5, 5306, 2012.
- 612 Meagher, J. F., Stockburger, L., Bailey, E. M., and Huff, O.: The oxidation of sulfur dioxide to sulfate aerosols in the plume
613 of a coal-fired power plant, *Atmos. Environ.*, 12, 11, 2197-2203, 1978.
- 614 Mercado, L. M. Bellouin, N. Sitch, S. Boucher, O. Huntingford, C. Wild, M. and Cox, P. M.: Impact of changes in diffuse
615 radiation on the global land carbon sink, *Nature*, 458, 7241, 1014-1017, 2009.
- 616 Miao, Y. C., Liu, S. H., Zheng, Y. J., Wang, S., Liu, Z. X., and Zhang, B. H.: Numerical study of the effects of planetary
617 boundary layer structure on the pollutant dispersion within built-up areas, *J. Environ. Sci.*, 32, 168-179, 2015a.
- 618 Miao, Y. C., Hu, X. M., Liu, S. H., Qian, T., Xue, M., Zheng, Y., and Wang, S.: Seasonal variation of local atmospheric
619 circulations and boundary layer structure in the Beijing-Tianjin-Hebei region and implications for air quality, *J. Adv.
620 Model. Earth Syst.*, 7, 1, 1-25, 2015b.
- 621 Miao, Y. C., Guo, J. P., Liu, S. H., Liu, H., Zhang, G., Yan, Y., and He, J.: Relay transport of aerosols to Beijing-Tian-Hebei
622 region by multi-scale atmospheric circulations, *Atmos. Environ.*, 165, 35-45, 2017a.
- 623 Miao, Y. C., Guo, J. P., Liu, S. H., Liu, H., Li, Z. Q., Zhang, W. C., and Zhai, P. M.: Classification of summertime synoptic
624 patterns in Beijing and their associations with boundary structure affecting aerosol pollution, *Atmos. Chem. Phys.*, 17,
625 3097-3110, 2017b.
- 626 Ministry of Environmental Protection of China (MEP), Ambient air quality standards (GB 3095–2012), 12 pp., China
627 Environmental Science Press, Beijing, 2012 (in Chinese).
- 628 Oh, I. B., Kim, Y. K., Lee, H. W., and Kim, C. H.: An observational and numerical study of the effects of the late sea breeze
629 on ozone distributions in the Busan metropolitan area, Korea, *Atmos. Environ.*, 40, 1284-1298, 2006.
- 630 Palm, B. B., Campuzano-Jost, P., Day, D. A., Ortega, A. M., Fry, J. L., Brown, S. S., Zarzana, K. J., Dube, W., Wagner, N.
631 L., Draper, D. C., Kaser, L., Jud, W., Karl, T., Hansel, A., Gutiérrez-Montes, C., and Jimenez, J. L.: Secondary organic
632 aerosol formation from in situ OH, O₃, and NO₃ oxidation of ambient forest air in an oxidation flow reactor, *Atmos.
633 Chem. Phys.*, 17, 5331-5354, 2017.
- 634 Parrish, D. D., Hahn, C. J., Williams, E. J., Borton, R. B., Fehsenfeld, F. C., Singh, H. B., Shetter, J. D., Gandrud, B. W., and
635 Ridley, B. A.: Indications of photochemical histories of Pacific air masses from measurements of atmospheric trace
636 species at Point Arena, California, *J. Geophys. Res.*, 97, 15883-15901, 1992.
- 637 Parrish, D. D., Trainer, M., Holloway, J. S., Yee, J. E., Warshawsky, M. S., and Fehsenfeld, F. C.: Relationships between
638 ozone and carbon monoxide at surface sites in the North Atlantic region, *J. Geophys. Res.*, 103, 13357-13376, 1998.
- 639 Polissar, A.V., Hopke, P.K., Paatero, P., Kaufmann, Y.J., Hall, D.K., Bodhaine, B.A., Dutton, E.G. and Harris, J.M.: The
640 aerosol at Barrow, Alaska: long-term trends and source locations. *Atmos. Environ.*, 33, 2441-2458, 1999.
- 641 Pope, C. and Dockery, D.: Epidemiology of particle effects. In *Air pollution and health*; Holgate, S. T., Koren, H. S., Samet,
642 J. M., Maynard, R. L., Eds.; Academic Press: San Diego, 1999; 673-705.



- 643 Poppe, D., Wallasch, M., and Zimmermann, J.: The dependence of the concentration of OH on its precursors under
644 moderately polluted conditions: a model study, *J. Atmos. Chem.*, 16, 61-78, 1993.
- 645 Qi, B., Du, R., Yu, Z., Zhou, B., and Yuan, X.: Characteristics of atmospheric fine particles concentrations in Hangzhou
646 region, *Environ. Chem.*, 34, 77-82, 2015.
- 647 Qi, H. X., Lin, W. L., Xu, X. B., Yu, X. M., and Ma, Q. L.: Significant downward trend of SO₂ observed from 2005 to 2010
648 at a background station in the Yangtze Delta region, China, *Sci. China Chem.*, 55, 7, 1451-1458, 2012.
- 649 Ravishankara, A. R.: Heterogeneous and multiphase chemistry in the troposphere, *Science*, 276, 1058-1065, 1997.
- 650 Roelofs, G. J. and Lelieveld, J.: Model study of the influence of cross-tropopause O₃ transports on tropospheric O₃ levels,
651 *Tellus B*, 49, 38-55, 1997.
- 652 Saxena, P. and Seigneur, C.: On the oxidation of SO₂ to sulfate in atmospheric aerosols, *Atmos. Environ.*, 21, 4, 807-812,
653 1987.
- 654 Seinfeld, J. H., Carmichael, G. R., Arimoto, R., Conant, W. C., Brechtel, F. J., Bates, T. S., Cahill, T. A., Clarke, A. D.,
655 Doherty, S. J., Flatau, P. J., Huebert, B. J., Kim, J., Markowicz, K. M., Quinn, P. K., Russell, L. M., Russell, P. B.,
656 Shimizu, A., Shinzuka, Y., Song, C. H., Tang, Y. H., Uno, I., Vogelmann, A. M., Weber, R. J., Woo, J. H., and Zhang,
657 X. Y.: ACE-ASIA - Regional climatic and atmospheric chemical effects of Asian dust and pollution. *Bull. Am.*
658 *Meteorol. Soc.*, 85, 3, 367-380, 2004.
- 659 Seinfeld, J. H. and Pandis, S. N.: *Atmospheric Chemistry and Physics: From Air Pollution to Climate Change*, 2nd ed., John
660 Wiley & Sons: New York, USA, 57-58 and 381-383, 2006
- 661 Seltenrich, N.: A clearer picture of China's air using satellite data and ground monitoring to estimate PM_{2.5} over time,
662 *Environ. Health Persp.*, 124, A38, 2016.
- 663 Shao, M., Tang, X. Y., Zhang, Y. H., and Li, W. J.: City clusters in China: air and surface water pollution, *Front. Ecol.*
664 *Environ.*, 4, 7, 353-361, 2006.
- 665 Sillman, S.: Ozone production efficiency and loss of NO_x in power plant plumes: photochemical model and interpretation of
666 measurements in Tennessee, *J. Geophys. Res.*, 105, 9189-9202, 2000.
- 667 Streets, D. G. and Waldhoff, S. T.: Present and future emissions of air pollutants in China: SO₂, NO_x, and CO, *Atmos.*
668 *Environ.*, 34, 3, 363-374, 2000.
- 669 Streets, D. G., Fu, J. S., Jang, C. J., Hao, J. M., He, K. B., Tang, X. Y., Zhang, Y. H., Wang, Z. F., and Li, Z. P.: Air quality
670 during the 2008 Beijing Olympic Games, *Atmos. Environ.*, 41, 480-492, 2007.
- 671 Su, S., Li, B. G., Cui, S. Y., Tao, S.: Sulfur dioxide emissions from combustion in China: from 1990 to 2007, *Environ. Sci.*
672 *Technol.*, 45, 8403-8410, 2011
- 673 Sun, G., Yao, L., Jiao, L., Shi, Y., Zhang, Q., Tao, M., Shan, G., and He, Y.: Characterizing PM_{2.5} pollution of a subtropical
674 metropolitan area in China, *Atmos. Climate. Sci.*, 3, 11, 2013.
- 675 Trainer, M., Parrish, D. D., Buhr, M. P., Norton, R. B., Fehsenfeld, F. C., Anlauf, K. G., Bottenheim, J. W., Tang, Y. Z.,
676 Wiebe, H. A., Roberts, J. M., Tanner, R. L., Newman, L., Bowersox, V. C., Meagher, J. F., Olszyna, K. J., Rodgers, M.



- 677 O., Wang, T., Berresheim, H., Demerjian, K. L., and Roychowdhury, U. K.: Correlation of O₃ with NO_y in
678 photochemically aged air, *J. Geophys. Res.*, 98, 2917-2925, 1993.
- 679 Wang, R., Tao, S., Ciais, P., Shen, H. Z., Huang, Y., Chen, H., Shen, G. F., Wang, B., Li, W., Zhang, Y. Y., Lu, Y., Zhu, D.,
680 Chen, Y. C., Liu, X. P., Wang, W. T., Wang, X. L., Liu, W. X., Li, B. G., and Piao, S. L.: High-resolution mapping of
681 combustion processes and implications for CO₂ emissions, *Atmos. Chem. Phys.*, 13, 10, 5189-5203, 2013.
- 682 Wang, G., Huang, L., Gao, S., Gao, S., and Wang, L.: Characterization of water-soluble species of PM₁₀ and PM_{2.5} aerosols
683 in urban area in Nanjing, China, *Atmos. Environ.*, 36, 1299-1307, 2002.
- 684 Wang, G., Wang, H., Yu, Y., Gao, S., Feng, J., Gao, S., and Wang, L.: Chemical characterization of water-soluble
685 components of PM₁₀ and PM_{2.5} atmospheric aerosols in five locations of Nanjing, China, *Atmos. Environ.*, 37, 2893-
686 2902, 2003.
- 687 Wang, T., Cheung, V. T. F., Anson, M., and Li, Y. S.: Ozone and related gaseous pollutants in the boundary layer of eastern
688 China: overview of the recent measurements at a rural site, *Geophys. Res. Lett.*, 28, 2373-2376, 2001.
- 689 Wang, T., Wong, C. H., Cheung, T. F., Blake, D. R., Arimoto, R., Baumann, K., Tang, J., Ding, G. A., Yu, X. M., Li, Y. S.,
690 Streets, D. G., and Simpson, I. J.: Relationships of trace gases and aerosols and the emission characteristics at Lin'an, a
691 rural site in eastern China, during spring 2001, *J. Geophys. Res.*, 109, 19, 2004.
- 692 Wang, Y., Ying, Q., Hu, J., and Zhang, H.: Spatial and temporal variations of six criteria air pollutants in 31 provincial
693 capital cities in China during 2013-2014, *Environ. Int.*, 73, 413-422, 2014.
- 694 Wang, Y. Q., Zhang, X. Y., Arimoto, R., Cao, J. J., and Shen, Z. X.: The transport pathways and sources of PM₁₀ pollution
695 in Beijing during spring 2001, 2002 and 2003, *Geophys. Res. Lett.*, 31, L14110, 2004.
- 696 Wu, J., Xu, C., Wang, Q., and Cheng, W.: Potential sources and formations of the PM_{2.5} pollution in urban Hangzhou,
697 *Atmosphere*, 7, 100, 2016a.
- 698 Wu, Y., Hu, M., Zeng, L., Dong, H., Li, X., Lu, K., Lu, S., Yang, Y., and Zhang, Y.: Seasonal variation of trace gas
699 compounds and PM_{2.5} observed at an urban supersite in Beijing, *EGU General Assembly Conference Abstracts*, 12409,
700 2016b.
- 701 Xu, H. H., Pu, J. J., He, J., Liu, J., Qi, B., and Du, R.-G.: Characteristics of atmospheric compositions in the background area
702 of Yangtze River Delta during heavy air pollution episode, *Adv. Meteor.*, 1-13, 2016.
- 703 Xue, L. K., Wang, T., Gao, J., Ding, A. J., Zhou, X. H., Blake, D. R., Wang, X. F., Saunders, S. M., Fan, S. J., Zuo, H. C.,
704 Zhang, Q. Z., and Wang, W. X.: Ground-level ozone in four Chinese cities: precursors, regional transport and
705 heterogeneous processes, *Atmos. Chem. Phys.*, 14, 13175-13188, 2014.
- 706 Yang, L. X., Cheng, S. H., Wang, X. F., Nie, W., Xu, P. J., Gao, X. M., Yuan, C., and Wang, W. X.: Source identification
707 and health impact of PM_{2.5} in a heavily polluted urban atmosphere in China, *Atmos. Environ.*, 75, 265-269, 2013.
- 708 Yu, S. C., Zhang, Q. Y., Yan, R. C., Wang, S., Li, P. F., Chen, B. X., Liu, W. P., and Zhang, X. Y.: Origin of air pollution
709 during a weekly heavy haze episode in Hangzhou, China, *Environ. Chem. Lett.*, 12, 543-550, 2014.



- 710 Zhang, H. L., Li, J. Y., Ying, Q., Yu, J. Z., Wu, D., Cheng, Y., He, K. B., and Jiang, J. K.: Source apportionment of PM_{2.5}
711 nitrate and sulfate in China using a source-oriented chemical transport model, *Atmos. Environ.*, 62, 228-242, 2012.
- 712 Zhang, L. M., Gong, S. L., Padro, J., and Barrie, L.: A size segregated particle dry deposition scheme for an atmospheric
713 aerosol module, *Atmos. Environ.*, 35, 549-560, 2001.
- 714 Zhang, R, Jing, J., Tao, J., Hsu, S. C., Wang, G., Cao, J., Lee, C. S. L., Zhu, L., Chen, Z., Zhao, Y., and Shen, Z.: Chemical
715 characterization and source apportionment of PM_{2.5} in Beijing: seasonal perspective, *Atmos. Chem. Phys.*, 13, 7053-
716 7074, 2013.
- 717 Zhang, R. Y., Suh, I., Zhao, J., Zhang, D., Fortner, E. C., Tie, X. X., Molina, L. T., and Molina, M. T.: Atmospheric new
718 particle formation enhanced by organic acids, *Science*, 304, 5676, 1487-1490, 2004.
- 719 Zhang, Q., Yuan, B., Shao, M., Wang, X., Lu, S., Lu, K., Wang, M., Chen, L., Chang, C.-C., and Liu, S. C.: Variations of
720 ground-level O₃ and its precursors in Beijing in summertime between 2005 and 2011, *Atmos. Chem. Phys.*, 14, 6089-
721 6101, 2014.
- 722 Zhang, Q., Streets, D. G., Carmichael, G. R., He, K. B., Huo, H., Kannari, A., Klimont, Z., Park, I. S., Reddy, S., Fu, J. S.,
723 Chen, D., Duan, L., Lei, Y., Wang, L. T., and Yao, Z. L.: Asian emissions in 2006 for the NASA INTEX-B mission,
724 *Atmos. Chem. Phys.*, 9, 5131-5153, 2009.
- 725 Zhong, Q. R., Huang, Y., Shen, H. Z., Chen, Y. L., Chen, H., Huang, T. B., Zeng, E. Y., and Tao, S.: Global estimates of
726 carbon monoxide emissions from 1960 to 2013, *Environ. Sci. Pollut. Res.*, 24, 864-873, 2014.
- 727



728 Table 1 Statistics of general meteorological parameters at NRCS for the period during January- December 2013*.

Month	Temperature (°C)	RH (%)	Wind Speed (m s ⁻¹)	Rainfall (mm)	Pressure (Pa)	Visibility (m)
Jan.	4.5	76	1.9	24.9	10221.6	2566.0
Feb.	7.0	81	2.3	66.8	10197.2	3511.8
Mar.	12.3	67	2.7	115.9	10140.5	5459.1
Apr.	16.9	56	2.6	98.1	10095.3	7587.8
May	23	69	2.1	121.3	10045.8	6118.9
Jun.	24.7	78	2.0	346	10013.0	5693.5
Jul.	32.2	51	2.8	9.3	9997.8	17011.0
Aug.	31.3	58	2.6	212.1	10001.7	13958.3
Sep.	24.5	73	2.3	49.4	10015.2	9584.7
Oct.	19	73	2.5	331	10146.1	7551.8
Nov.	13.5	68	1.9	32.6	10178.8	5759.2
Dec.	6.3	64	2.0	82.7	10208.6	3941.2

729 *Note: average values for air temperature (T), relative humidity (RH), wind speed (WS), pressure, and visibility and
 730 accumulated monthly value for rainfall, respectively.

731



732 Table 2 Mean species levels for different seasons and different time of day and comparisons with other previous data
 733 reported in typical regions in China.

Species	Areas	Location	Period	The whole day			Day time (08:00-17:00)			Night time (18:00-07:00)		
				Mean	SD	Max	Mean	SD	Max	Mean	SD	Max
PM _{2.5} ($\mu\text{g m}^{-3}$)	This study	YRD	DJF	74.2	49.3	406.4	75.1	50.5	406.4	73.6	48.4	325.5
			MAM	47.1	26.2	201.1	47.7	26.6	201.1	46.7	25.9	154.0
			JJA	34.6	22.5	181	35.1	25.7	181.0	34.3	20.0	139.6
			SON	52.5	34.4	272.4	51.7	33.3	238.1	53.1	35.1	272.4
	YRD	PRD	^a Xiacheng District, Hangzhou (Sep.-Nov. 2013) monthly mean: $69 \mu\text{g m}^{-3}$									
			^b NRCS, Hangzhou (2012) annual mean: $50.0 \mu\text{g m}^{-3}$									
			^c Hangzhou (Sep. 2010-Nov. 2011 during non-raining days) annual average: $106\text{-}131 \mu\text{g m}^{-3}$									
			^d Nine sites in Nanjing (2013) AM: $55\text{-}60 \mu\text{g m}^{-3}$, JJA: $30\text{-}60 \mu\text{g m}^{-3}$, SON: $55\text{-}85 \mu\text{g m}^{-3}$									
	YRD	BTH	^e Nanjing (Mar. 2013-Feb. 2014) annual mean: $75 \pm 50 \mu\text{g m}^{-3}$									
			^e Shanghai (Mar. 2013-Feb. 2014) annual mean: $56 \pm 41 \mu\text{g m}^{-3}$									
			^e Beijing (Mar. 2013-Feb. 2014) annual mean: $87 \pm 67 \mu\text{g m}^{-3}$									
			^e Guangzhou (Mar. 2013-Feb. 2014) annual mean: $52 \pm 28 \mu\text{g m}^{-3}$									
PM ₁₀ ($\mu\text{g m}^{-3}$)	This study	YRD	DJF	113.1	71.7	589.6	115.3	73.6	589.6	111.5	70.4	481.6
			MAM	77.1	42.3	484.1	79.3	41.0	249.1	75.6	43.2	484.1
			JJA	54.9	31.6	231.4	55.7	34.8	231.4	54.4	29.2	183.8
			SON	85.6	51.2	344.2	84.8	48.6	341.3	86.1	53.0	344.2
	YRD	PRD	^e Hangzhou (Mar. 2013-Feb. 2014) annual mean: $98 \pm 59 \mu\text{g m}^{-3}$									
			^c Hangzhou (Sep. 2010-Nov. 2011 during non-raining days) annual average: $127\text{-}158 \mu\text{g m}^{-3}$									
			^f Hangzhou (Sep. 2001-Aug. 2002) annual mean: $119.2 \mu\text{g m}^{-3}$									
			^e Nanjing (Mar. 2013-Feb. 2014) annual mean: $134 \pm 73 \mu\text{g m}^{-3}$									
	YRD	BTH	^e Shanghai (Mar. 2013-Feb. 2014) annual mean: $80 \pm 47 \mu\text{g m}^{-3}$									
			^e Beijing (Mar. 2013-Feb. 2014) annual mean: $109 \pm 62 \mu\text{g m}^{-3}$									
			^e Guangzhou (Mar. 2013-Feb. 2014) annual mean: $72 \pm 35 \mu\text{g m}^{-3}$									
O ₃ (ppbv)	This study	YRD	DJF	13.8	13.1	70.9	17.7	14.1	70.9	10.2	10.9	58.5
			MAM	29.8	24.0	141.2	42.4	27.3	141.2	20.0	15.1	105.9
			JJA	31.3	26.0	145.4	48.8	26.6	145.4	18.2	15.8	118.7
			SON	25.9	22.5	100.1	37.0	25.1	100.1	16.3	14.3	99.5
	YRD	PRD	^e Hangzhou (Mar. 2013-Feb. 2014) annual mean: $44 \pm 21 \text{ ppbv}$ (8 h O ₃)									
			^e Nanjing (Mar. 2013-Feb. 2014) annual mean: $42 \pm 20 \text{ ppbv}$ (8 h O ₃)									
			^e Shanghai (Mar. 2013-Feb. 2014) annual mean: $48 \pm 21 \text{ ppbv}$ (8 h O ₃)									
			^e Beijing (Mar. 2013-Feb. 2014) annual mean: $45 \pm 27 \text{ ppbv}$ (8 h O ₃)									
	YRD	BTH	^e Guangzhou (Mar. 2013-Feb. 2014) annual mean: $45 \pm 24 \text{ ppbv}$ (8 h O ₃)									
SO ₂ (ppbv)	YRD	This study	DJF	14.5	10.2	71.2	16.2	10.2	71.2	13.3	10.2	64.6



		MAM	11.3	9.1	75.1	11.7	9.6	75.1	11.0	8.7	59.3	
		JJA	8.6	6.5	51.0	8.0	6.3	51.0	9.0	6.6	46.7	
		SON	9.6	7.2	63.8	10.3	7.1	58.3	9.0	7.3	63.8	
		^a Hangzhou Xiacheng District (12-19 Oct., 2013) daily mean: 5.7-9.7 ppbv										
		^e Hangzhou (Mar. 2013-Feb. 2014) annual mean: 9 ± 4 ppbv										
		^e Nanjing (Mar. 2013-Feb. 2014) annual mean: 12 ± 6 ppbv										
		^e Shanghai (Mar. 2013-Feb. 2014) annual mean: 7 ± 5 ppbv										
	BTH	^e Beijing (Mar. 2013-Feb. 2014) annual mean: 9 ± 8 ppbv										
	PRD	^e Guangzhou (Mar. 2013-Feb. 2014) annual mean: 7 ± 3 ppbv										
CO (ppmv)	YRD	DJF	1.4	0.7	3.8	1.4	0.7	3.3	1.4	0.7	3.8	
		This study	MAM	0.7	0.2	2.2	0.7	0.3	2.2	0.7	0.2	1.7
			JJA	0.5	0.2	2.0	0.5	0.2	1.9	0.5	0.2	2.0
			SON	0.8	0.3	3.4	0.7	0.3	1.9	0.8	0.3	3.4
		^e Hangzhou (Mar. 2013-Feb. 2014) annual mean: 0.7 ± 0.3 ppmv										
		^e Nanjing (Mar. 2013-Feb. 2014) annual mean: 0.8 ± 0.4 ppmv										
		^e Shanghai (Mar. 2013-Feb. 2014) annual mean: 0.7 ± 0.3 ppmv										
	BTH	^e Beijing (Mar. 2013-Feb. 2014) annual mean: 1.1 ± 0.7 ppmv										
	PRD	^e Guangzhou (Mar. 2013-Feb. 2014) annual mean: 0.8 ± 0.2 ppmv										
	NO ₂ (ppbv)	YRD	DJF	37.4	20.1	146.9	35.7	19.5	126.3	38.5	20.5	146.9
This study			MAM	28.7	12.9	94.8	25.3	12.1	94.8	31.0	12.9	87.4
			JJA	17.3	10.2	61.4	13.0	9.2	46.1	20.3	9.7	61.4
			SON	28.4	15.2	94.1	25.1	13.3	86.2	30.7	16.0	94.1
		^e Hangzhou (Mar. 2013-Feb. 2014) annual mean: 13 ± 9 ppbv										
		^e Nanjing (Mar. 2013-Feb. 2014) annual mean: 26 ± 11 ppbv										
		^e Shanghai (Mar. 2013-Feb. 2014) annual mean: 20 ± 9 ppbv										
BTH		^e Beijing (Mar. 2013-Feb. 2014) annual mean: 25 ± 11 ppbv										
PRD		^e Guangzhou (Mar. 2013-Feb. 2014) annual mean: 24 ± 10 ppbv										
NO _x (ppbv)		YRD	DJF	60.5	34.7	199.8	58.0	32.1	168.9	62.3	36.3	199.8
	This study		MAM	40.0	19.8	131.4	36.5	19.2	129.2	42.5	19.8	131.4
			JJA	24.3	14.8	99.6	18.6	14.1	99.6	28.2	14.0	83.1
			SON	41.0	24.3	153.4	36.6	21.1	123.7	44.2	25.8	153.4
NO _y (ppbv)	YRD	DJF	84.7	48.4	295.2	82.4	44.6	263.7	86.4	51.1	295.2	
		This study	MAM	66.0	33.6	248.8	62.9	34.6	248.8	68.2	32.8	204.1
			JJA	43.6	27.6	259.5	36.8	29.3	259.5	48.5	25.2	167.7
			SON	70.2	37.9	319.3	65.5	35.6	319.3	73.6	39.1	251.8
	^g Nanjing SORPES 2013 monthly mean: 30-70 ppbv											
	^h Shanghai May-June 2005 daily mean: 24-39 ppbv											



BTH ^a Beijing 2011-2015 annual mean: 54.6 ± 4.7 ppbv

YRD ^h Guangzhou Apr.-May 2004: 24-52 ppbv

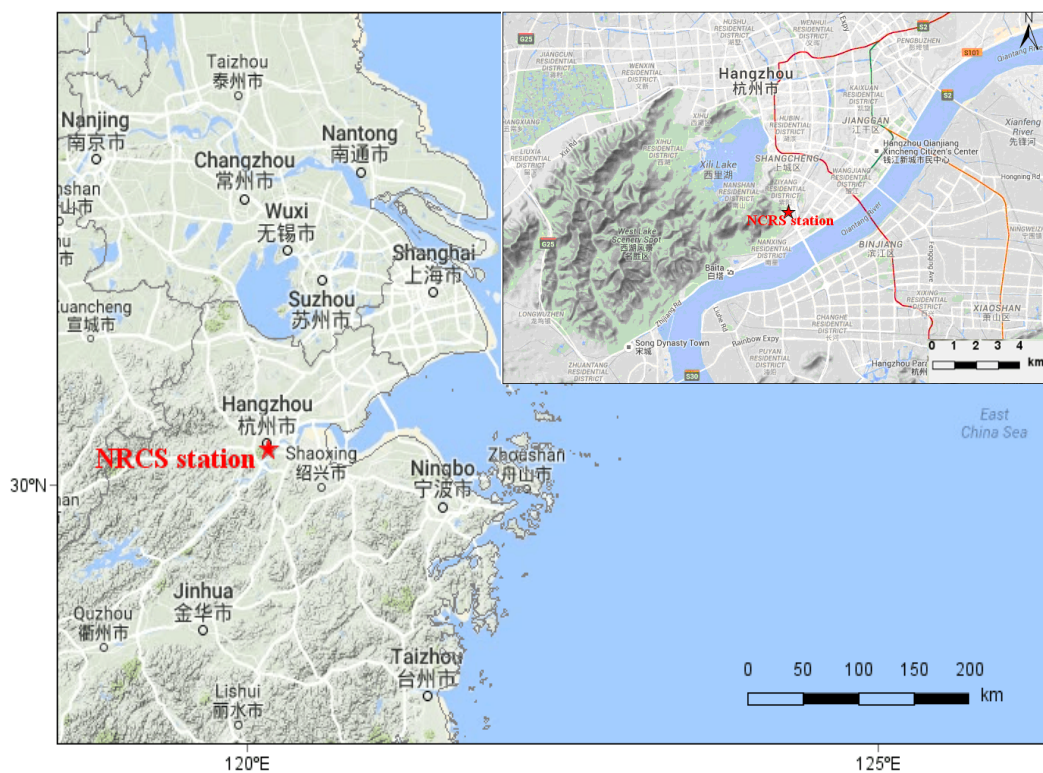
734 ^a Wu et al. (2016a); ^b Qi et al. (2015); ^c Sun et al. (2013); ^d Chen et al. (2016); ^e Wang et al. (2014); ^f Cao et al. (2009); ^g Ding

735 et al. (2013); ^h Xue et al. (2014)



736 Table 3 Mean concentrations of PM_{2.5} (µg m⁻³) and other trace gases (ppmv unit for CO but ppbv for other gases) in the
 737 identified trajectory clusters within four season period, together with the percentages of each trajectory cluster.

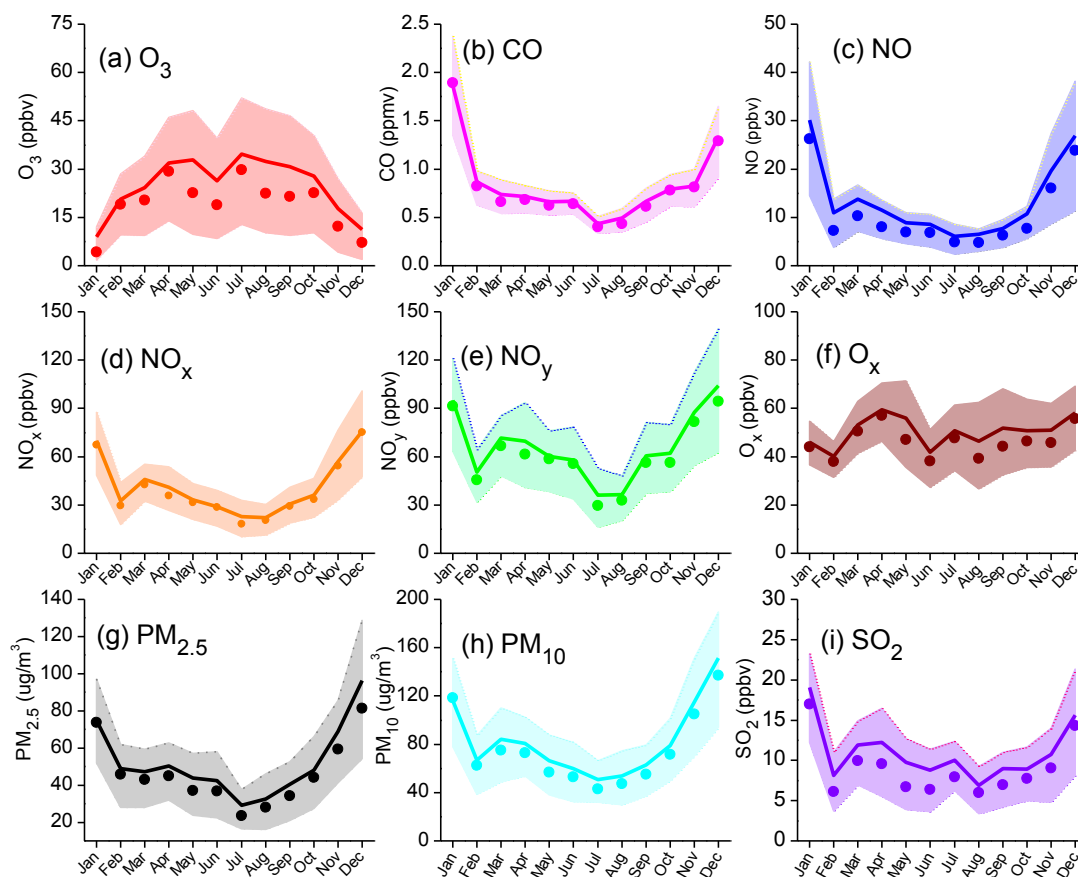
Season	Cluster	Percent (%)	PM _{2.5}	O ₃	SO ₂	CO	NO _x
Spring	1	12.05	45.0	28.3	10.7	0.7	38.3
	2	16.58	44.3	31.6	13.2	0.7	39.1
	3	16.03	35.3	30.5	9.7	0.6	34.5
	4	42.66	52.4	23.2	11.4	0.8	42.5
	5	5.53	38.2	34.2	11.2	0.7	37.9
	6	7.16	58.1	34.2	11.9	0.8	43.8
Summer	1	8.42	51.5	24.6	7.9	0.8	29.2
	2	8.61	34.2	35.2	9.2	0.5	22.8
	3	22.55	24.0	28.7	7.9	0.4	21.7
	4	31.34	38.2	36.8	9.1	0.5	24.4
	5	19.38	38.7	27.2	8.9	0.6	28.7
	6	9.69	22.4	26.7	7.5	0.4	17.6
Autumn	1	23.63	42.1	27.4	9.9	0.7	36.9
	2	32.51	50.7	24.6	8.2	0.8	39.4
	3	8.33	21.7	19.8	8.0	0.5	22.0
	4	7.78	68.6	34.8	8.4	0.8	38.8
	5	11.90	49.9	22.6	10.1	0.7	40.8
	6	15.84	79.6	21.6	12.9	0.9	62.0
Winter	1	7.13	60.9	16.6	15.4	1.3	53.7
	2	24.26	83.3	14.4	15.9	1.4	65.4
	3	16.39	47.3	14.0	11.9	1.1	42.7
	4	21.76	75.9	11.9	13.5	1.5	63.1
	5	16.76	67.0	11.7	13.1	1.5	53.7
	6	13.70	102.1	14.4	16.9	1.4	81.0



738

739

Fig. 1. Location of NRCS station in YRD region (left) and in the city of Hangzhou (right top).



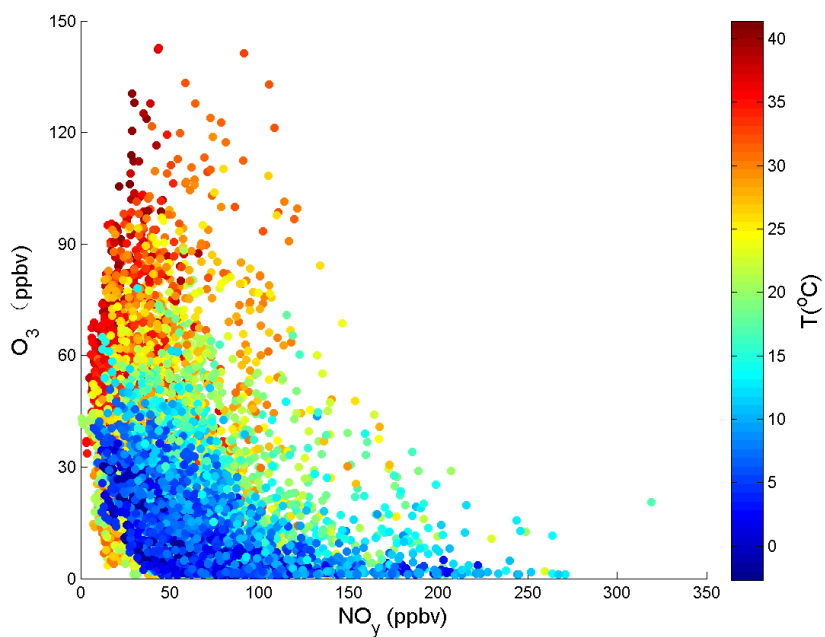
740

741 Fig. 2. Seasonal variations of atmospheric O₃ (a), CO (b), NO (c), NO_x (d), NO_y (e), O_x (f), PM_{2.5} (g), PM₁₀ (h), and SO₂ (i).

742 Bold solid lines are the monthly averages, solid circles are the median values, and thin lines represent percentiles of 75% and

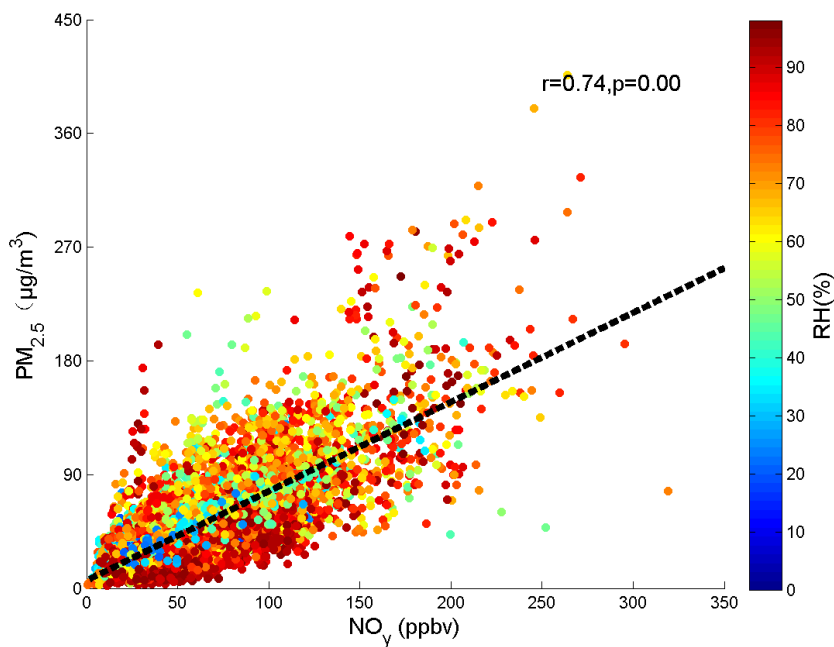
743

25%.



744
745

Fig. 3. Scatter plots of NO_y with O_3 coded with air temperature



746
747

Fig. 4. Scatter plots of NO_y with $\text{PM}_{2.5}$ coded with relative humidity

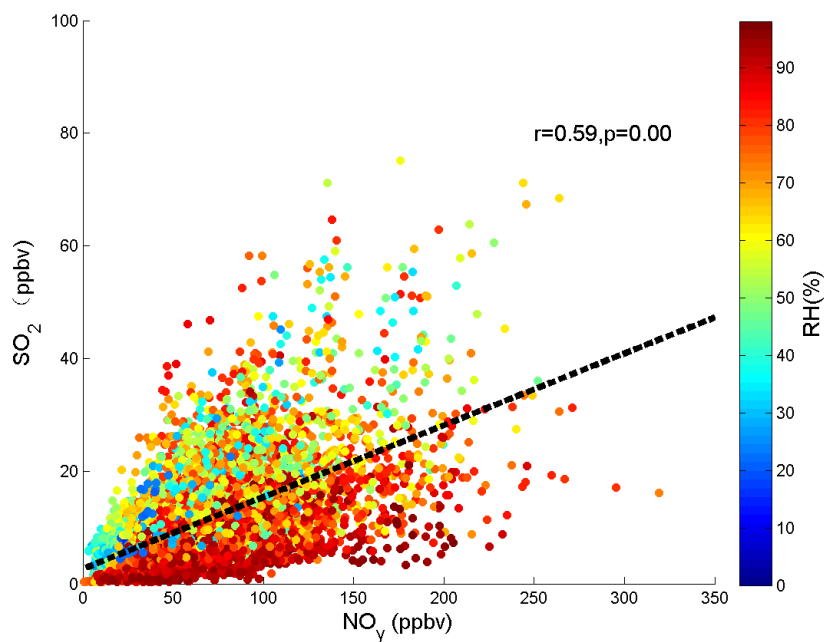


Fig. 5. Scatter plots of NO_y with SO_2 coded with relative humidity

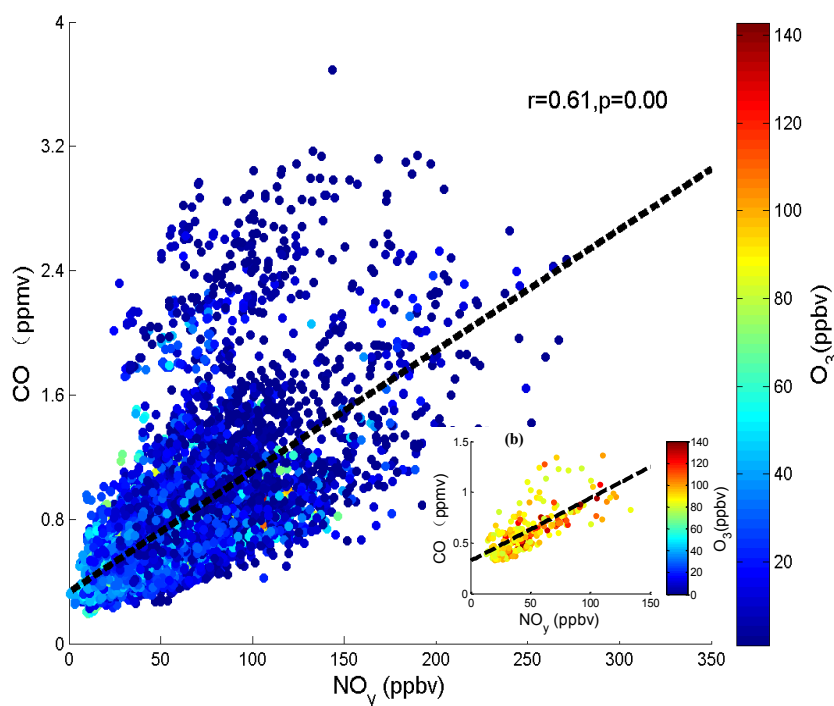


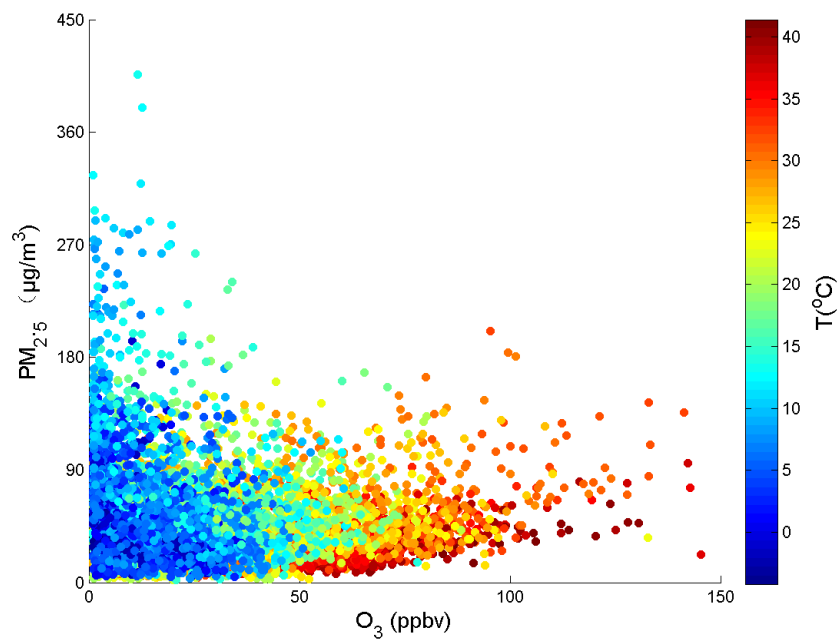
Fig. 6. Scatter plots of NO_y with CO coded with O_3 mixing ratios, along the subpicture (b) showing the scatter with O_3 mixing ratios above 80 ppbv.

748
749
750

751
752
753



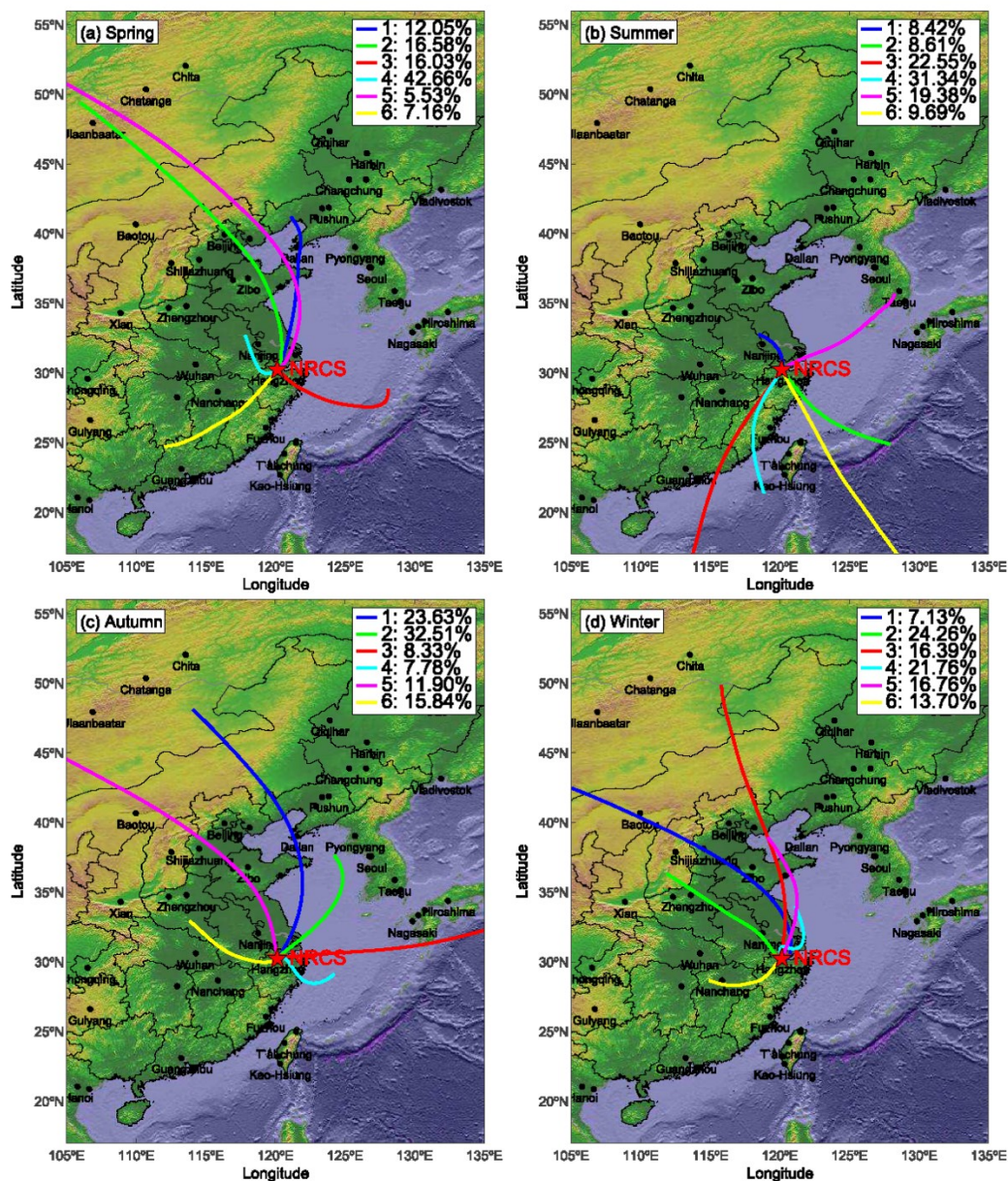
754



755

756

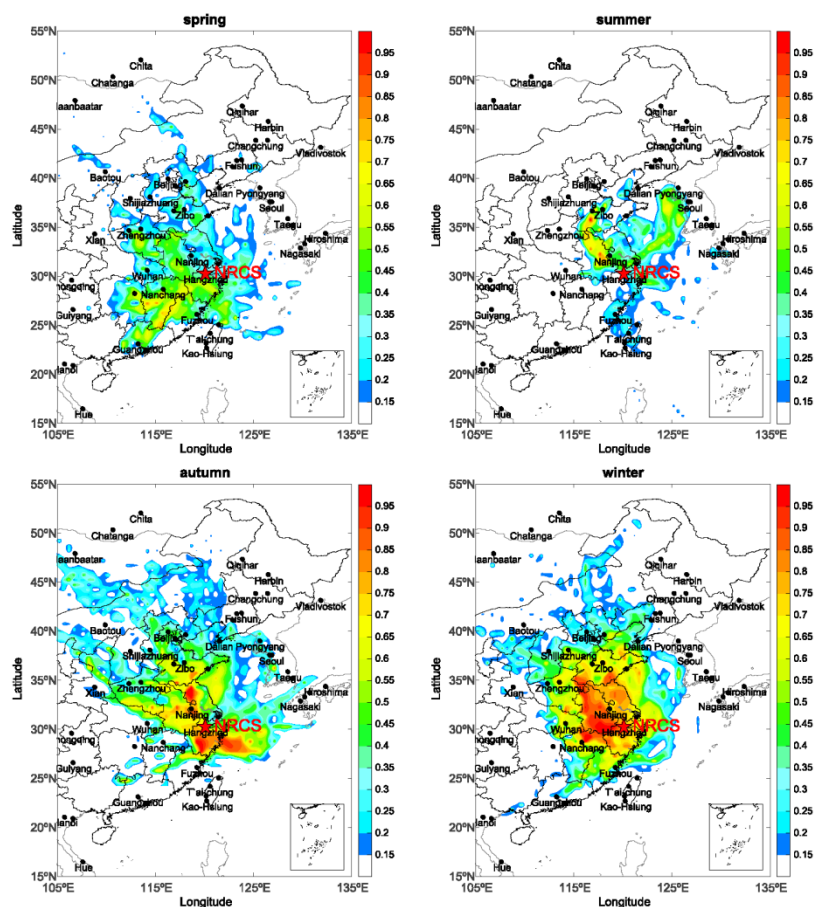
Fig. 7. Scatter plots of O₃ with PM_{2.5} coded with air temperature



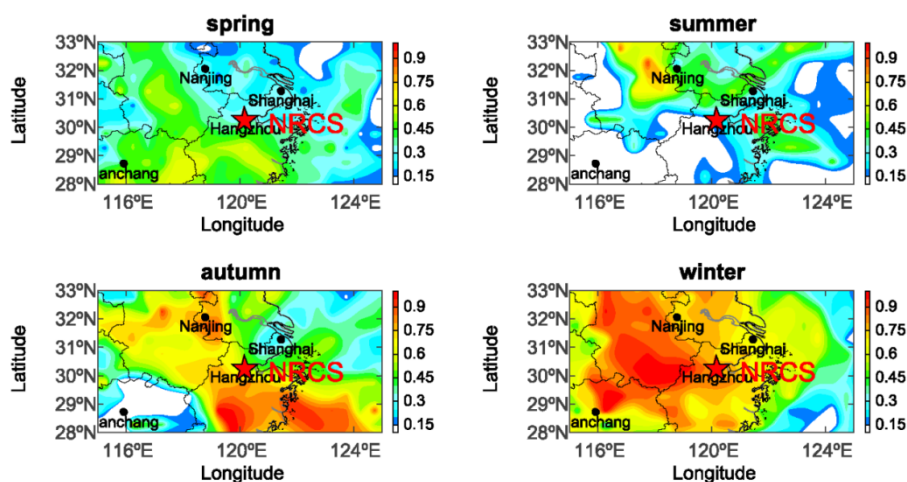
757

758

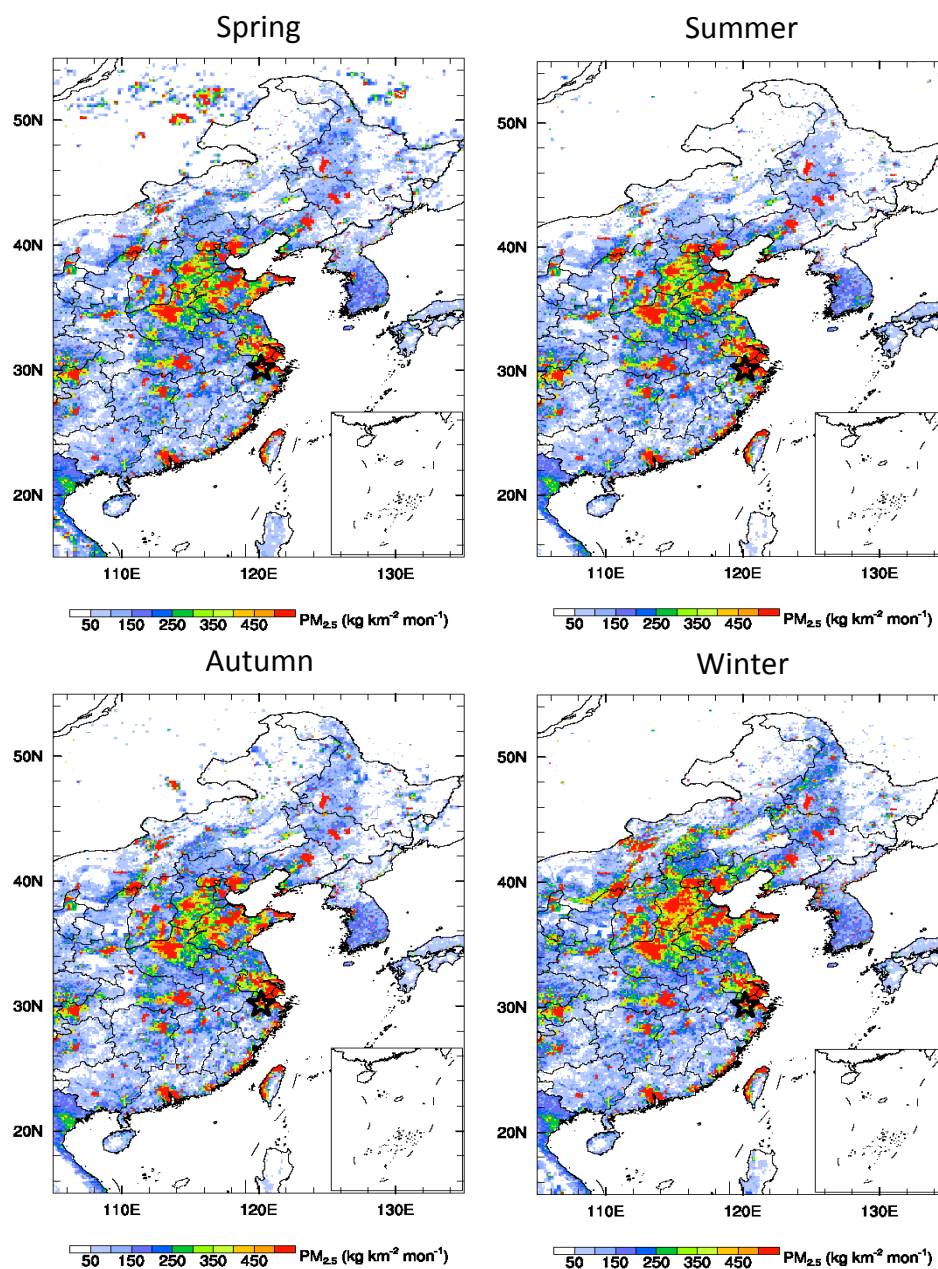
Fig. 8. Seasonal cluster analysis of the 72-h air mass back trajectories starting at 100 m from NRCS site in Hangzhou.



759
 760 Fig. 9a. Seasonal weighted potential source contribution function (WPSCF) maps of PM_{2.5} in Hangzhou. The sampling site is
 761 marked in pentacle and the WPSCF values are displayed in color.



762
 763 Fig. 9b. The zoomed view of Fig. 9a.



764

765 Fig. 9c. Seasonal and spatial distributions of PM_{2.5} emissions (kg km² mon⁻¹) at the surface layer in China. The sampling site

766

is marked in pentacle.

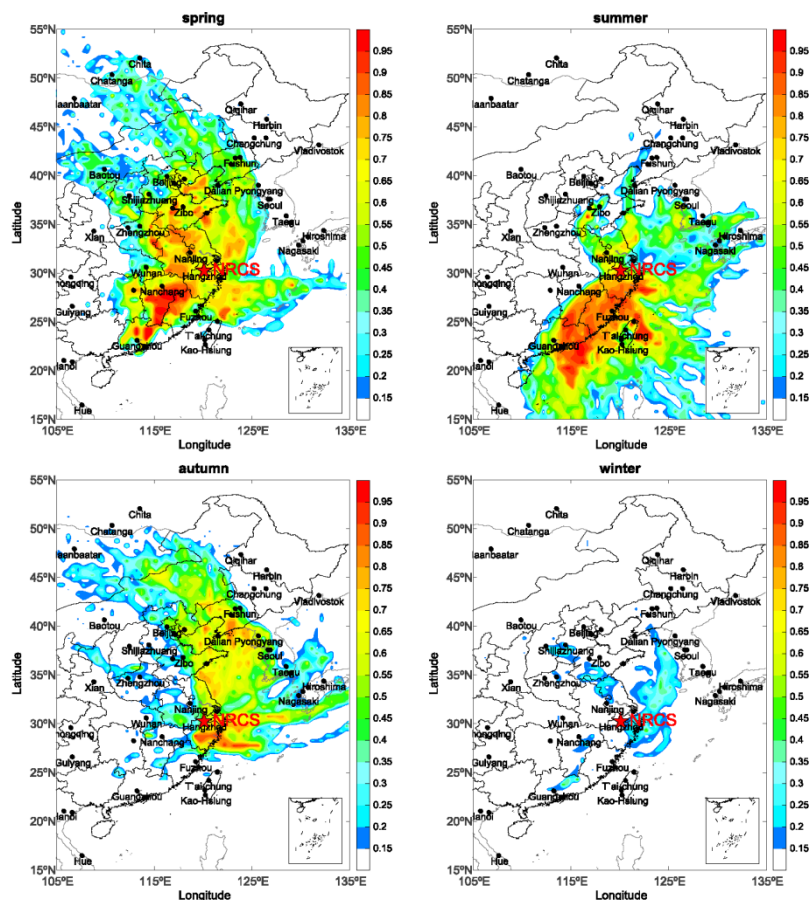


Fig. 10a. Same as Fig. 9a but for O₃

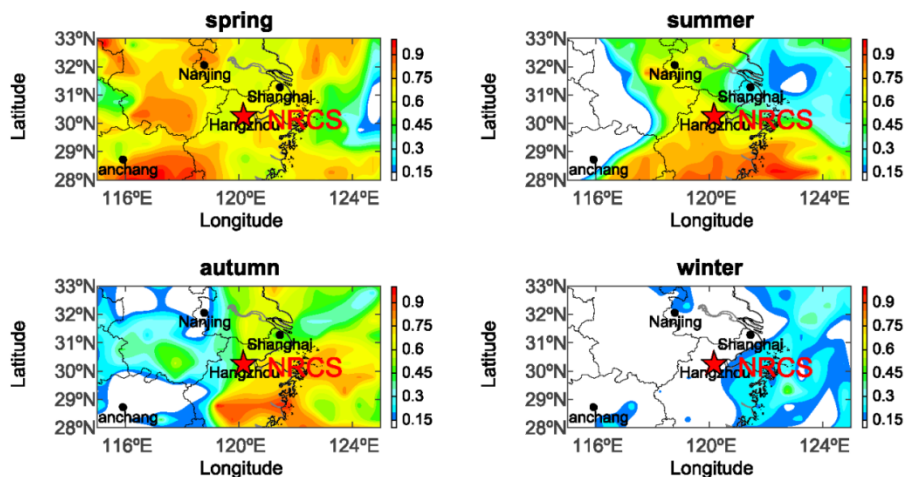


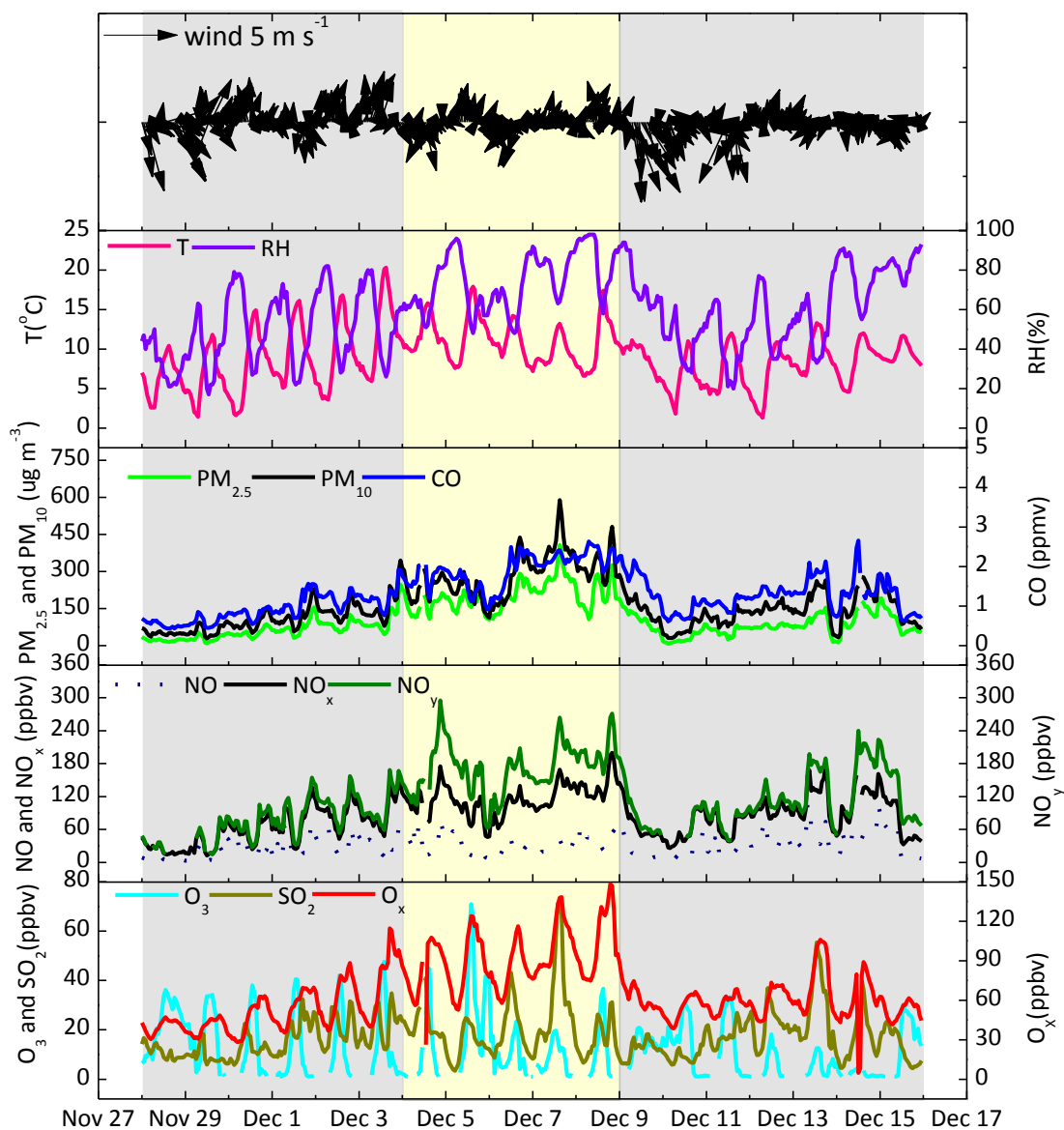
Fig. 10b The zoomed view of Fig. 10a

767

768

769

770



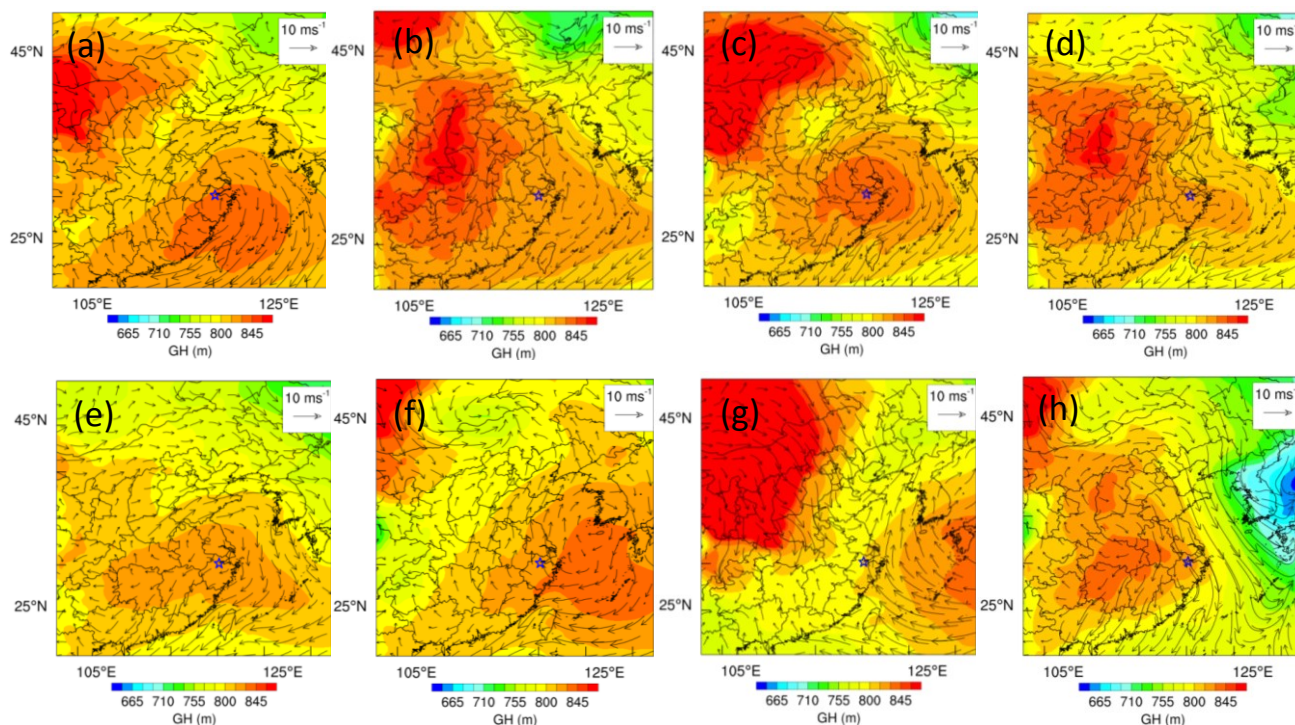
771

772

773

774

Fig. 11. Time series of meteorological parameters and chemical species before, during, and after haze period. The gray shaded area indicates the Phase I (28 Nov.-3 Dec.) and II (10-12 Dec.) and the orange shaded area represents haze events Phase III (2-9 Dec.) and IV (13-15 Dec.).

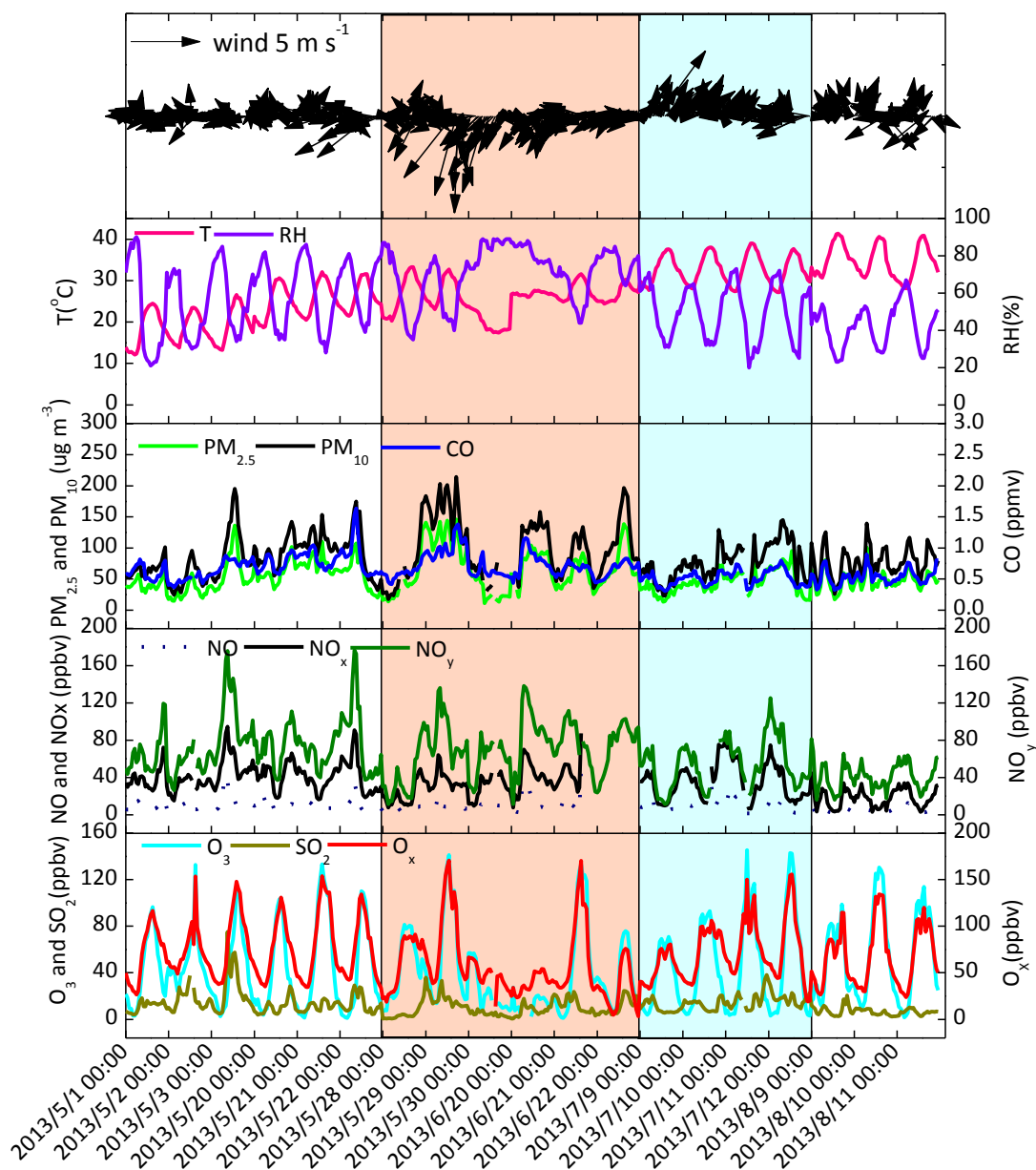


775

776 Fig. 12. The Geopotential Height Field (GH) (indicated by color bars) and Wind Field (WF) (black vectors) for 925 hPa at

777 20:00 LT during 2-9 December, 2013. Fig. 12a-d and Fig. 12e-h represent for 2-5 December and 6-9 December from left to

778 right on the top and bottom, respectively. The NRCS station was marked by pentagram.



779

780 Fig. 13. Same as Fig. 11 but during photochemical pollution period. The orange shaded area represents the Phase I (28-30
 781 May and 20-22 June), the cyan shaded area indicates the Phase II (9-12 July), and the other area represents the Phase III (1-3
 782 May, 20-22 May, and 9-11 August)